Journal of Geophysical Research: Oceans

RESEARCH ARTICLE
10.1029/2018JC014074

North Atlantic Ocean Internal Decadal Variability: Role of the Mean State and Ocean-Atmosphere Coupling

Guillaume Gastineau[1], **Juliette Mignot**[1], **Olivier Arzel**[2], **and Thierry Huck**[2]

[1]LOCEAN, Sorbonne Université/CNRS/IRD/MNHN, Paris, France, [2]LOPS, UMR 6523 CNRS/IFREMER/IRD/UBO, Brest, France

Key Points:
- The AMOC and AMV decadal variability can emerge from a self-sustained oceanic mode based on coupled model results
- Increasing atmospheric resolution decreases the oceanic variability due to mean state changes
- Atmosphere-ocean coupling causes a moderate increase of the AMOC variability

Supporting Information:
- Supporting Information S1

Correspondence to:
G. Gastineau,
guillaume.gastineau@upmc.fr

Citation:
Gastineau, G., Mignot, J., Arzel, O., & Huck, T. (2018). North Atlantic Ocean internal decadal variability: Role of the mean state and ocean-atmosphere coupling. *Journal of Geophysical Research: Oceans*, *123*. https://doi.org/10.1029/2018JC014074

Received 12 APR 2018
Accepted 24 JUL 2018
Accepted article online 6 AUG 2018

Abstract The origin of the decadal variability in the North Atlantic Ocean is investigated in a series of coupled and ocean-only numerical experiments. Two versions of the IPSL-CM5A model are considered, differing only by their atmospheric horizontal resolution (3.75° × 1.87° and 2.5° × 1.25°). When the ocean model is forced by the climatological surface fluxes from the low atmospheric resolution coupled model version, a 20-year variability emerges, similar to the variability found in the coupled simulation. Such decadal variability is consistent with a large-scale baroclinic instability of the mean flow in the west European basin. Increasing the atmospheric resolution leads to a more intense Icelandic low, which intensifies the western subpolar gyre, and warms the eastern North Atlantic subpolar gyre region. The mean state changes nearly vanish the associated internal oceanic variability under the corresponding climatological surface fluxes. Increasing the atmospheric resolution also produces a slightly weaker atmospheric stochastic forcing. Both the mean state and atmospheric variability changes are consistent with the decreasing amplitude of the variability in the coupled model. For both model versions, the amplitude of the internal oceanic variability is strongly enhanced in the presence of atmospheric stochastic forcing. Air-sea coupling on the other hand has a moderate influence on the amplitude of the variability only in the low-resolution model version, where the North Atlantic oceanic variability at 20 years increases by 23% due to coupling. The coupling effect is therefore modest and sensitive to the atmospheric horizontal resolution.

1. Introduction

The Atlantic Meridional Overturning Circulation (AMOC) is a major component of the climate system, as it transports tremendous amounts of heat northward. It has a major influence on the climate of the continents surrounding the Atlantic Ocean, as shown by models (Stouffer et al., 2006; Swingedouw et al., 2009; Vellinga & Wood, 2002; Jackson et al., 2015) and paleoclimate studies (Clark et al., 2002; Rahmstorf, 2002). A deeper understanding of the AMOC variability also has important socioeconomic benefit, as the AMOC might be predictable at decadal time scales (Keenlyside et al., 2008).

The AMOC is difficult to observe, and a continuous monitoring only exists from 2005 onward (McCarthy et al., 2012; Mercier et al., 2015; Smeed et al., 2014), so that models have been extensively used to understand its decadal variability. In global climate models, the AMOC shows an important natural variability with decadal to centennial time scales in control runs using constant forcings for the greenhouse gases, aerosols, or ozone. The AMOC variability might explain why the subpolar North Atlantic is the region where predictability at lead time of 2 to 5 years is the largest compared to other basins in models (Meehl et al., 2014; Mignot et al., 2016). Some models show no preferred time scale (Kwon & Frankignoul, 2012), while others show two dominant time scales for the AMOC decadal variability (Frankcombe et al., 2010). The interplay between the AMOC and the freshwater balance of the Arctic Ocean has been suggested to be at the origin of a 50- to 70-year time scale in models (Frankcombe & Dijkstra, 2011; Jungclaus et al., 2005). Such variability dominates for the sea surface temperature (SST) during the instrumental period (Knight et al., 2006). A shorter 20- to 30-year variability is also apparent at subpolar latitudes of the North Atlantic Ocean in observations (Chylek et al., 2011; Frankcombe & Dijkstra, 2009; Plaut et al., 1995) and many models (Menary et al., 2015). Several idealized studies of the North Atlantic basin have suggested that the 20- to 30-year time scale is fixed by the transit time of unstable planetary waves propagating westward (Colin de Verdière & Huck, 1999; Sévellec & Fedorov, 2010; Te Raa & Dijkstra, 2002). The present study focuses on the IPSL (Institut Pierre Simon Laplace) models (IPSL-CM5A-LR which uses a relatively low atmospheric horizontal resolution 3.75° × 1.87° and IPSL-CM5A-MR based on a slightly higher atmospheric resolution 2.5° × 1.25°) that show such 20-year variability (Escudier et al., 2013; Muir & Fedorov, 2017; Ortega et al., 2015; Wen et al., 2016). What the

precise role is of air-sea coupling and atmospheric stochastic forcing in these models, remains to be determined. The intent of this paper is to serve as a continuation of the previous works realized with the IPSL models by addressing these central questions.

The processes responsible for the AMOC decadal climate variability were reported to be due to (1) the atmospheric stochastic forcing (Frankignoul & Hasselmann, 1977; Delworth & Greatbatch, 2000), (2) self-sustained oceanic intrinsic variability (Arzel et al., 2018; Sérazin et al., 2016), or (3) coupled mode of variability (Timmermann et al., 1998). Most low-resolution ocean models show little variability when using bulk formulation as surface boundary condition (Danabasoglu et al., 2014). However, the use of salinity restoring and the uncertainties in bulk formulations might have some crucial effect on the AMOC decadal variability in such simulations. On the other hand, idealized models using prescribed surface fluxes can generate a decadal oceanic intrinsic variability (Colin de Verdière & Huck, 1999; Jamet et al., 2016). Furthermore, Delworth and Greatbatch (2000) have shown that most of the AMOC variability can be produced by atmospheric stochastic forcing. The main mode of North Atlantic SST multidecadal variability, referred to as AMV (Atlantic multidecadal variability), was reported to be mainly influenced by the atmosphere (Cane et al., 2017; Clement et al., 2015; Schneider & Fan, 2007). These results are nevertheless under debate because the AMOC northward heat transport was also identified as a driver of the AMV (Zhang, 2017), and in many models AMOC intensification leads to a warm AMV phase with a time lag ranging from 1 to 9 years (Muir & Fedorov, 2015). Therefore, the relative role of the atmospheric forcing for the AMV is not yet fully understood compared to that of ocean dynamics, and this study aims at better quantifying it in a coupled model.

Lastly, the oceanic circulation could also have an impact on the large-scale atmospheric modes of variability. In many models, the SST and sea ice anomalies related to the AMOC or the AMV may cause a significant atmospheric response albeit weak (Gastineau & Frankignoul, 2012; Peings et al., 2016; Peings & Magnusdottir, 2014). For instance, in IPSL-CM5A-LR, a negative and eastward shifted North Atlantic Oscillation (NAO) pattern occurs as a response to the subpolar SST anomalies (Gastineau et al., 2016), and the positive phase of the NAO was also found to increase the AMOC a few years later (Gastineau & Frankignoul, 2012), so that the coupling may have a positive feedback for the 20-year AMOC variability. In IPSL-CM5A-MR, which differs from IPSL-CM5A-LR by the higher atmospheric resolution, the AMOC was reported to have a different atmospheric response (Wen et al., 2016). It was argued that the AMOC induces a simultaneous NAO anomaly, acting in turn as a strong positive feedback onto the AMOC variability. The Atlantic gyre circulation may also play a role for the coupling together with the AMOC (Bellucci et al., 2008; Fan & Schneider, 2012; Gastineau et al., 2013). However, ocean-atmosphere coupling in models was mostly investigated using statistical analyses of control coupled simulation, where causes and consequences are difficult to distinguish. The last objective of the present study is to unravel the role of ocean-atmosphere coupling using targeted model simulations.

In the following, we use the ocean component of the IPSL model and investigate and quantify the processes giving rise to the AMOC and AMV variability. We show that the North Atlantic exhibits a 20-year variability originating from an internal oceanic mode. The characteristics of the variability are shown to be sensitive to the atmospheric resolution. Lastly, experiments are designed to investigate the role of atmospheric stochastic forcing and ocean-atmosphere coupling on the decadal-scale variability.

The experimental protocol and the model characteristics are presented in section 2. The internal oceanic mode of variability is identified and analyzed in section 3. The roles of atmospheric stochastic forcing and air-sea coupling are investigated in section 4. The paper concludes with a summary and a discussion.

2. Data and Methods

2.1. Coupled Model

This study uses the outputs of the IPSL-CM5A-LR and IPSL-CM5A-MR model CMIP5 (Coupled Model Intercompariason Project, phase 5) preindustrial control simulations (Dufresne et al., 2013), referred to as COUPLED-LR and COUPLED-MR in the following. Hereafter, we focus on periods of 500 years in COUPLED-LR and 300 years in COUPLED-MR, consistent with the periods used in Gastineau et al. (2013) and Wen et al. (2016) respectively.

Both COUPLED-LR and COUPLED-MR use the same ocean component, that is, the NEMOv3.2 ocean model with the ORCA2 grid (resolution of about 2°) and 31 vertical levels. These model versions use the LIM-2 sea ice component and the PISCES oceanic biogeochemistry model. The atmospheric component is the LMDZ-A model with the ORCHIDEE land surface module. The atmospheric model has 39 vertical levels and a horizontal resolution of 3.75° × 1.87° in COUPLED-LR and 2.5° × 1.25° in COUPLED-MR. Apart from the resolution, the two atmospheric configurations have the same physics and differ only by some of their tuning parameters.

The mean AMOC of the COUPLED simulations is weak, with a yearly mean value at 40°N of about 10 Sv in LR and 12 Sv in MR. This weak AMOC is linked to a cold bias that is present in both model versions at midlatitudes, with smaller amplitude in COUPLED-MR (−1.4 K in LR and −0.4 K in MR for the global land surface air temperature; Dufresne et al., 2013). The overextended sea ice inhibits the oceanic convection in the Labrador Sea, while it overestimates it south of Iceland (Escudier et al., 2013). Despite these deficiencies, the North Atlantic atmospheric variability in COUPLED-MR and COUPLED-LR was shown to be realistic (Cattiaux et al., 2013), with fairly realistic air-sea interactions (Gastineau et al., 2013). Both model versions show jet streams that are too far equatorward, but the improved resolution in COUPLED-MR leads to a more realistic location of the jet stream (Arakelian & Codron, 2012).

2.2. Ocean-Only Simulations

To investigate the North Atlantic variability, we perform several ocean-only experiments, using the same ocean component (NEMO) as in the coupled models but without using the sea ice (LIM2) and biogeochemistry (PISCES) modules. We use the NEMO version 3.6, using the same parameterization and parameters as the coupled simulations (see Dufresne et al., 2013 for details). The time-varying daily surface turbulent and radiative fluxes, the surface wind stress, and the freshwater fluxes (evaporation minus precipitation) are taken from the COUPLED simulations described above. The river runoff and sea ice concentration are set to a mean climatological field, both computed from COUPLED simulations. The sea ice concentration is prescribed with a simple representation of the heat and salt exchanges in the presence of sea ice. In case of sea ice, the SST is restored to the freezing point and a constant upward flux is added. The freshwater fluxes are modified so that the change in buoyancy fluxes remains negligible (Madec, 2015). Therefore, the ocean-only simulations investigated in the following do not consider sea ice-ocean interactions. Such interactions are important to reproduce realistic heat and salt exchanges between the North Atlantic and the Arctic, which can be dominant for the Atlantic multidecadal variability in other coupled models (i.e., Frankcombe & Dijkstra, 2011; Jungclaus et al., 2005).

To avoid any spurious drift and allow some damping of the surface anomalies, we use a weak surface restoring for temperature and salinity. Such temperature and salinity nudging are done via a Haney restoring term, where the strength of the nudging is set by the coefficient γ_S and γ_T (see Servonnat et al., 2015 for details in the restoring procedure). We use a relatively weak value of 10 $W{\cdot}m^{-2}{\cdot}K^{-1}$ for γ_T, which is smaller than the typical surface heat flux feedback inferred from observations over the North Atlantic (around 40 $W{\cdot}m^{-2}{\cdot}K^{-1}$, Frankignoul & Kestenare, 2002). The sea surface salinity (SSS) restoring coefficient γ_S is −50 mm/day, equivalent to a restoring time scale of 2.5 years for a 50 m mixed layer, much longer than typical values used in coordinated ocean-only simulations using bulk formula (Griffies et al., 2014).

The experiments follow the experimental protocol of Delworth and Greatbatch (2000). The first set of simulations, called CLIM, are integrated over 500 years, using a repeated cycle of daily climatological heat fluxes, wind stresses, and atmospheric freshwater fluxes computed from the COUPLED simulations. It is designed to quantify the internal ocean dynamics. In the second set of simulations, called TOTAL, the applied surface forcing consists in the daily time series of the daily surface fluxes from the COUPLED simulations. The TOTAL experiment is integrated over 500 years (300 years) for the LR (MR) case. To test the robustness of the results from TOTAL, we repeat this experiment with five different start dates using initial conditions sampled every 100 years from the first TOTAL run. The last set of simulations, called RANDOM, is designed to assess the impact of atmospheric stochastic forcing on the oceanic variability. The RANDOM experiments use randomly selected year from the TOTAL daily surface fluxes forcing. To account for time autocorrelation at interannual time scale, the selection of the year uses random permutations of 3-year blocks. This procedure was repeated three (six) times consecutively to derive the forcings of two simulations of 1,500 years (1,800 years) for the LR (MR) case. This procedure should

randomize the atmospheric forcing and attenuate any potential influence of the decadal frequencies included in the forcing from TOTAL. The ocean-only experiments CLIM, TOTAL, and RANDOM are repeated for the two model versions (LR and MR), to study the impact of atmospheric resolution. Unless stated otherwise, all runs are initialized from the initial state of the COUPLED runs.

2.3. Statistical Analysis and Climate Indices

To better highlight the decadal variability, we apply in the following a smoothing to several yearly time series. We use a low-pass Lanczos filter with a cutoff period of 10 years and 21 weights, or a band-pass Lanczos filter with 10 and 30 years as cutoff period and 31 weights. The amplitude of the variability is quantified with the standard deviation of the raw or filtered time series, after removal of a quadratic trend. When using raw yearly time series, the means and standard deviation of two simulations are compared using *t* test and *F* test, the effective number of degrees of freedom for yearly time series being determined following Bretherton et al. (1999). The level of significance for correlations is established using a *t* test, with the same method (Bretherton et al., 1999) to estimate the effective number of degrees of freedom. When using low-pass or band-pass time series, we find an *e*-folding time scale of about 7 years for most oceanic variables, so that the total degrees of freedom are estimated by the total number of years divided by 15 when comparing two standard deviations.

The AMOC strength is computed as the maximum between 500- and 2,000-m depth of the Atlantic meridional overturning stream function averaged in 40–55°N. As shown by Escudier et al. (2013), the precise choice of the region used to define the AMOC strength does not alter the results as long as the AMOC is evaluated within the subpolar gyre latitudes.

The surface signature of Atlantic Ocean variability is evaluated using the AMV time series and patterns. The AMV is defined as the Atlantic Ocean SST anomaly within 75°W–0°E and 0–60°N, smoothed by a low-pass Lanczos lowpass filter, using 10 years as a cutoff period. The AMV pattern is obtained by the SST regression onto the standardized AMV time series.

Lastly, we calculate the NAO index with an empirical orthogonal function analysis of the monthly sea level pressure (SLP) over the North Atlantic Ocean (100°W–40°E, 20–90°N). The NAO index is the standardized first principal component (PC). The NAO pattern is calculated as the SLP regression onto the NAO index. The East Atlantic pattern is calculated similarly but using the second PC.

2.4. Differences Between Coupled and Ocean-Only Simulations

The ocean-only model simulations cannot reproduce the results from the COUPLED runs, as the sea ice and biogeochemistry modules are deactivated, and as the ocean-only simulations use surface restoring conditions. We first compare the mean state and variability of the coupled and ocean-only experiments. The differences of the zonal mean Atlantic temperature and salinity between the COUPLED and CLIM runs do not exceed 0.4 K and 0.1 psu, irrespective of the model versions used (see supporting information Figure S1). In LR, some large temperature differences (~0.3 K) are located in the Arctic and Southern Oceans, presumably due to the different sea ice representation. In CLIM-MR, a large negative salinity anomaly is simulated at 20–55°N 1,000–2,500 m in the Atlantic Ocean. For both LR and LR we also note a warm (1 K) and salty (~0.2 psu) bias in the ocean-only runs located in the upper 500 m of the ocean at 45°N and, to a lesser extent, at 30°S. The tropics have a cold bias of about 0.4 K at 15°N–15°S only present in the upper 50 m. The mean North Atlantic SST over the AMV region is 18.7 °C for CLIM-LR and 19.7 °C for CLIM-MR, which is consistent with the results from the COUPLED simulations (18.5 °C and 19.5 °C, respectively). The mean state difference in TOTAL-LR shows a similar pattern but with larger amplitudes with typical maximum large-scale anomalies of ~0.5 K and ~0.1 psu below 500 m. TOTAL-MR shows again a fresh anomaly at 20–55°N more pronounced than in TOTAL-LR. The RANDOM simulations are similar to TOTAL (not shown).

Figure 1 illustrates the yearly AMOC variability in the COUPLED and TOTAL simulations. The AMOC averaged over 40–55°N in TOTAL-MR (9.30 Sv) is larger than TOTAL-LR (8.61 Sv), as expected from the corresponding coupled simulations. The amplitude of the AMOC variability is estimated by the standard deviation of the raw and low-pass time series (see numbers in Figure 1 and Table 1). As expected, the variability in TOTAL and COUPLED is similar (correlation $r = 0.83$ in LR, $r = 0.63$ in MR), but the amplitude is smaller in the ocean-only runs. The difference in mean value or standard deviation is larger between the TOTAL and COUPLED for the MR simulation, with an AMOC 1.5 Sv weaker in TOTAL from 2020 to 2280 and a larger

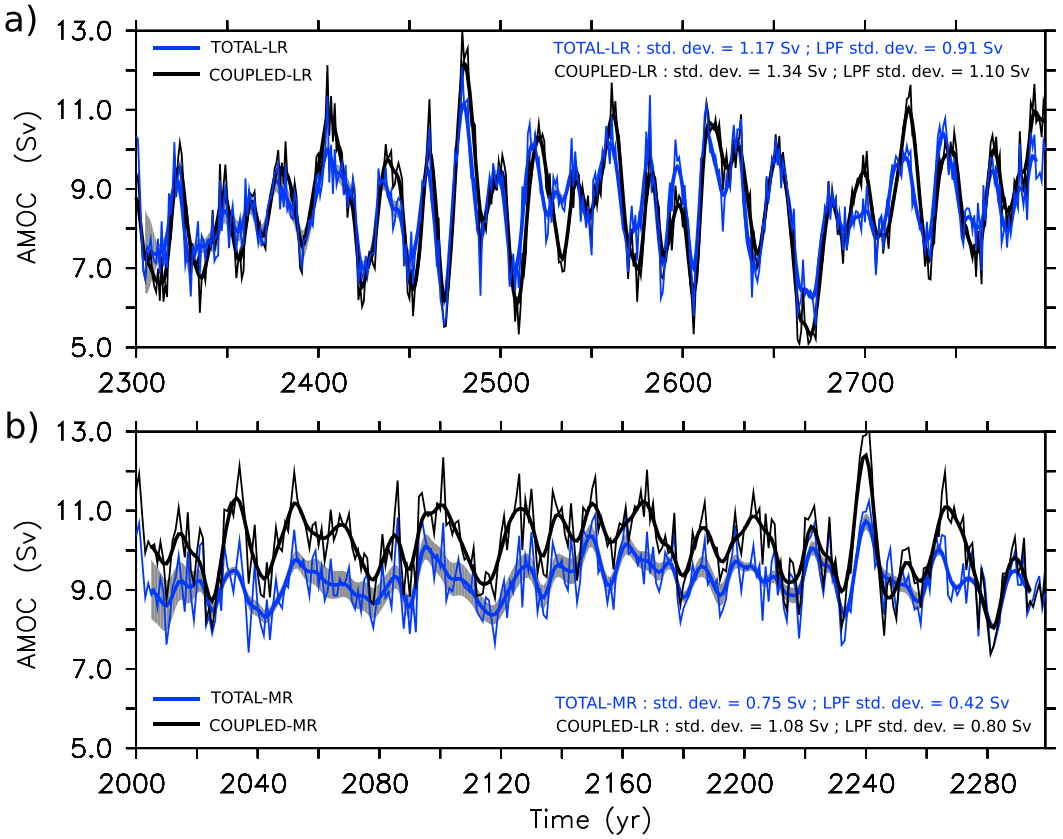

Figure 1. AMOC time series (Sv), for (a) the coupled simulation COUPLED-LR (black line) and the ocean-only simulation TOTAL-LR (blue line: ensemble mean; gray shades: standard deviation among members). (b) Same as (a) but for the COUPLED-MR and TOTAL-MR simulations. The standard deviation of yearly and low-pass filtered (LPF) time series is indicated in each panel. AMOC = Atlantic Meridional Overturning Circulation. See Table 1 and section 2.2 for simulation name and experimental protocol.

spread among the five ensemble members. The different behavior of the LR and MR versions is presumably linked to the different mean state bias, with a more intense fresh anomaly in the subpolar Atlantic in TOTAL-MR. This may be due to the impacts of the different surface boundary condition used and the missing sea ice interactions. Ocean-only runs under climatological surface fluxes (CLIM, Figure 2) also

Table 1
AMOC and North Atlantic Temperature Variability in the Coupled and Ocean-Only Simulations

Simulation	Surface boundary conditions	Model	AMOC standard deviation (Sv)		North Atlantic temperature standard deviation (10^{-1} K)
			Yearly	10–30 years	Yearly
COUPLED	Fully coupled	LR	1.35*	0.64	2.01
CLIM	Climatology	LR	0.32*	0.23*	0.35*
TOTAL	Raw daily fluxes	LR	1.12	0.64	1.86
RANDOM	Randomly selected daily fluxes	LR	1.04	0.52*	1.85
COUPLED	Fully coupled	MR	1.04*	0.43	1.73*
CLIM	Climatology	MR	0.09	0.03*	0.20*
TOTAL	Raw daily fluxes	MR	0.75	0.36	1.04
RANDOM	Randomly selected daily fluxes	MR	0.88*	0.42	1.22*

Note. The temperature variability is given by the standard deviation of the yearly subpolar North Atlantic (40–62°N; 75°W–0°E) potential temperature between 0 and 700 m. AMOC = Atlantic Meridional Overturning Circulation. LR and MR indicate if the simulations are based on the Low Resolution or Medium Resolution atmosphere, respectively.
*The level of significance is below 5% for the Fisher *F* test of the variances when compared to the corresponding TOTAL simulation.

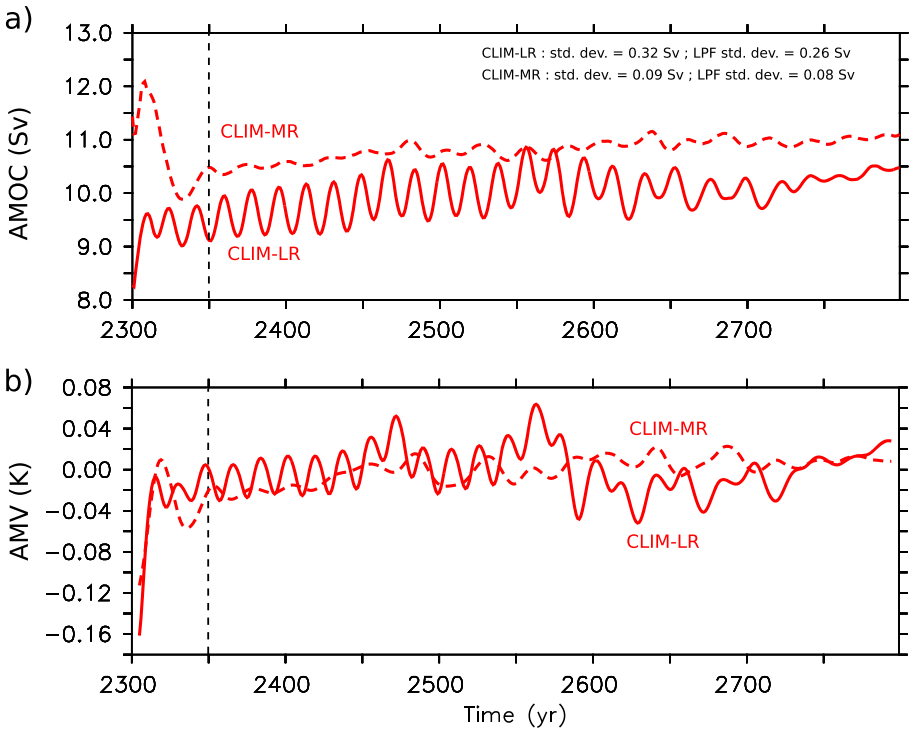

Figure 2. (a) AMOC (Sv), and (b) AMV (K), yearly time series for the ocean-only simulation forced by climatological fluxes CLIM-LR and CLIM-MR. No smoothing was applied to the time series. The standard deviation of yearly and low-pass filtered (LPF) time series is indicated in (a). AMOC = Atlantic Meridional Overturning Circulation; AMV = Atlantic multidecadal variability. See Table 1 and section 2.2 for simulation name and experimental protocol.

exhibit a significant but weak variability, with standard deviations in the AMOC low-pass index reaching only 29.1% and 10.0% of that obtained in COUPLED for the LR and MR runs respectively.

Figures 3a–3d show the standard deviation of the yearly upper ocean potential temperature averaged between 0 and 700 m depth, after removal of a quadratic drift in COUPLED and TOTAL. The overall spatial pattern of the COUPLED simulations is well captured in TOTAL, irrespective of the atmospheric horizontal resolution, with a weaker variance in MR than in LR (note difference in color bars). The agreement in terms of amplitude of temperature variability between COUPLED and TOTAL is, however, much better for the LR than the MR runs. In CLIM-LR, the temperature variance over the subpolar Atlantic basin shows a weak maximum in the subpolar Atlantic, centered at 55°N (Figure 3g). CLIM-MR (Figure 3h) has a weaker variance, but it still displays a broad maximum west of the mid-Atlantic Ridge in the Newfoundland Basin and downstream. In both CLIM simulations, the standard deviation is typically 20% to 30% that of the TOTAL simulation. RANDOM provides results similar to TOTAL and will be discussed later.

The SST signature of ocean variability is then illustrated using the AMV patterns in Figure 4. A horseshoe shaped pattern similar to that observed (Knight et al., 2006) with maximum amplitude over the subpolar basin is obtained in COUPLED at either low or medium atmospheric horizontal resolutions (Figures 4a and 4b). SST variations are larger at low resolutions. As expected from the use of SST restoring, the amplitude of the AMV is significantly reduced in ocean-only runs. However, the overall pattern in TOTAL remains comparable to that obtained in COUPLED (Figures 4c and 4d), with amplitudes of SST anomalies about half smaller. The AMV pattern in CLIM (Figures 4g and 4h) is even weaker than in TOTAL, but the maximum amplitude is still found in the subpolar gyre region. The amplitude is partly recovered in the RANDOM simulations, as will be commented later.

In summary, the ocean-only simulations forced by the surface fluxes diagnosed from the coupled models capture the region of maximum SST variance at subpolar latitudes but with a smaller amplitude than in the coupled models. In the following, we will use these ocean-only simulations to interpret the decadal variability produced in the coupled models.

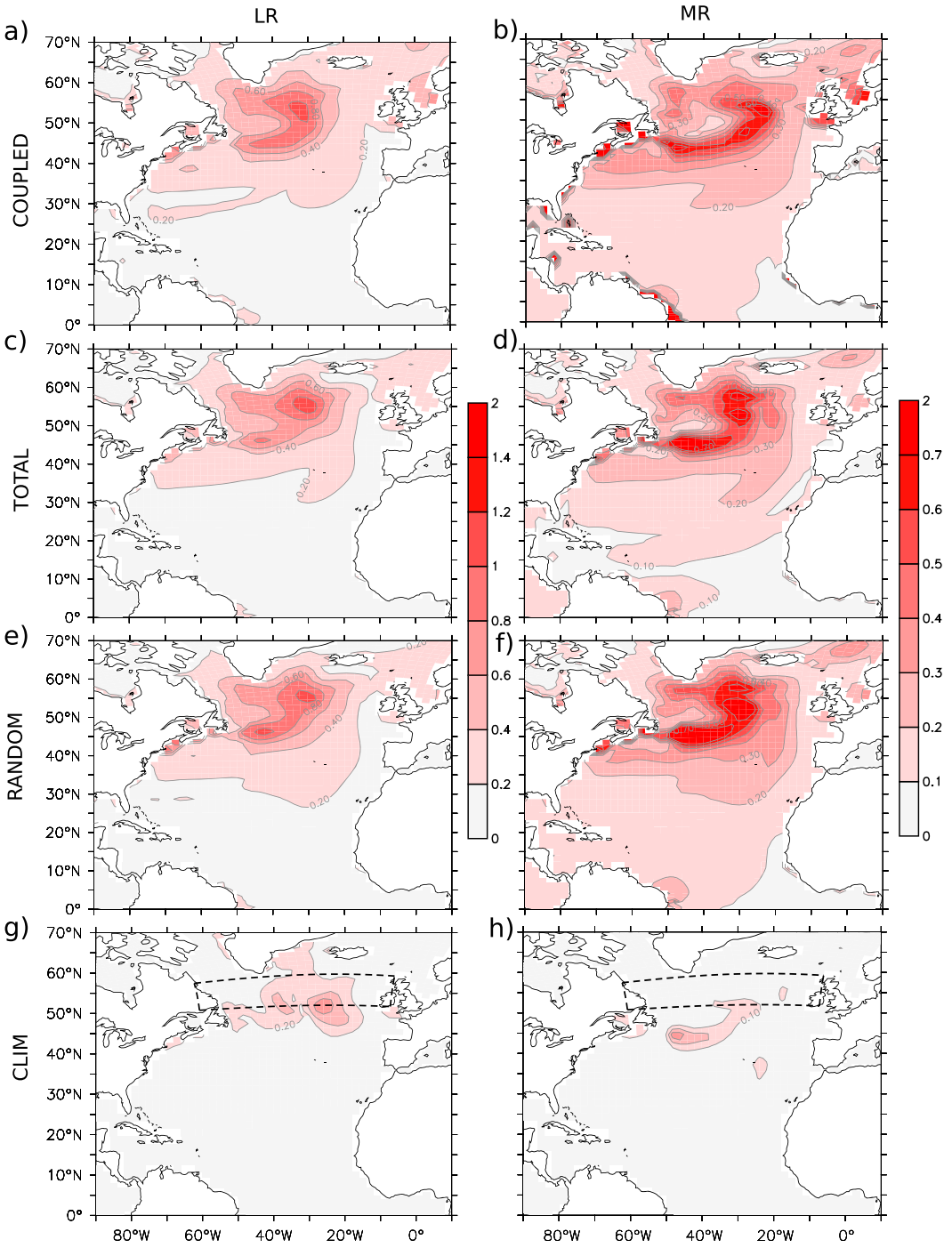

Figure 3. Standard deviation of the yearly mean potential temperature between 0 and 700 m, in kelvin, for (a) COUPLED-LR, (b) COUPLED-MR, (c) TOTAL-LR, (d) TOTAL-MR, (e) RANDOM-LR, (f) RANDOM-MR, (g) CLIM-LR, and (h) CLIM-MR. Note the difference in contour intervals in the left and right columns. The black dashed lines provide the location of the latitudinal band studied in Figure 6. See Table 1 and section 2.2 for simulation name and experimental protocol.

3. Oceanic Intrinsic Decadal Variability

3.1. Climatological Forcing

We first focus on the decadal variability produced in the ocean-only CLIM simulations using climatological flux forcing. The decadal variability generated in those runs is of interest as it is self-sustained and occurs

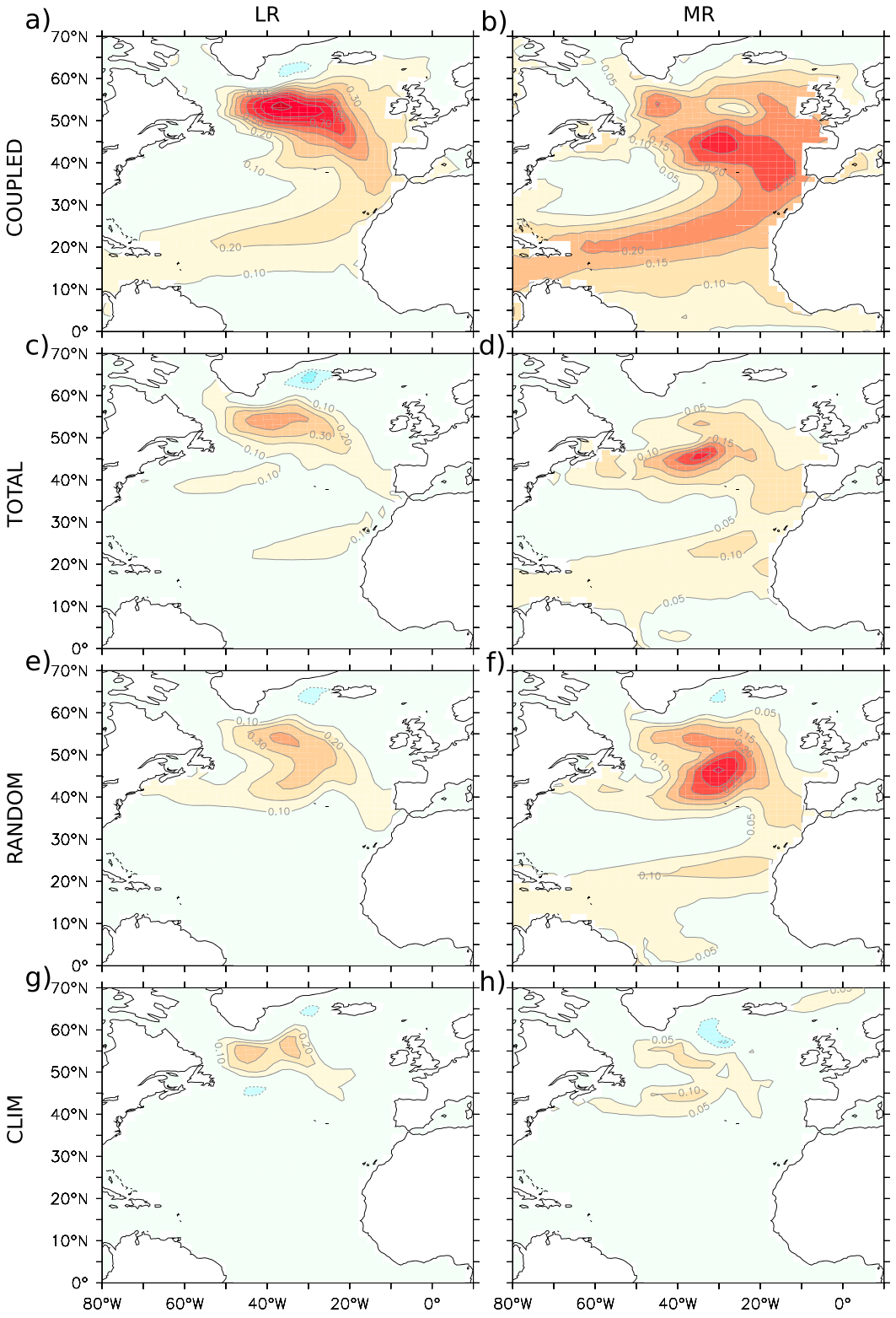

Figure 4. Atlantic multidecadal variability pattern (in kelvin/standard deviation) in (a) COUPLED-LR, (b) COUPLED-MR, (c) TOTAL-LR, (d) TOTAL-MR, (e) RANDOM-LR, (f) RANDOM-MR, (g) CLIM-LR, and (h) CLIM-MR. The contour interval is different in left and right columns. See Table 1 and section 2.2 for simulation name and experimental protocol.

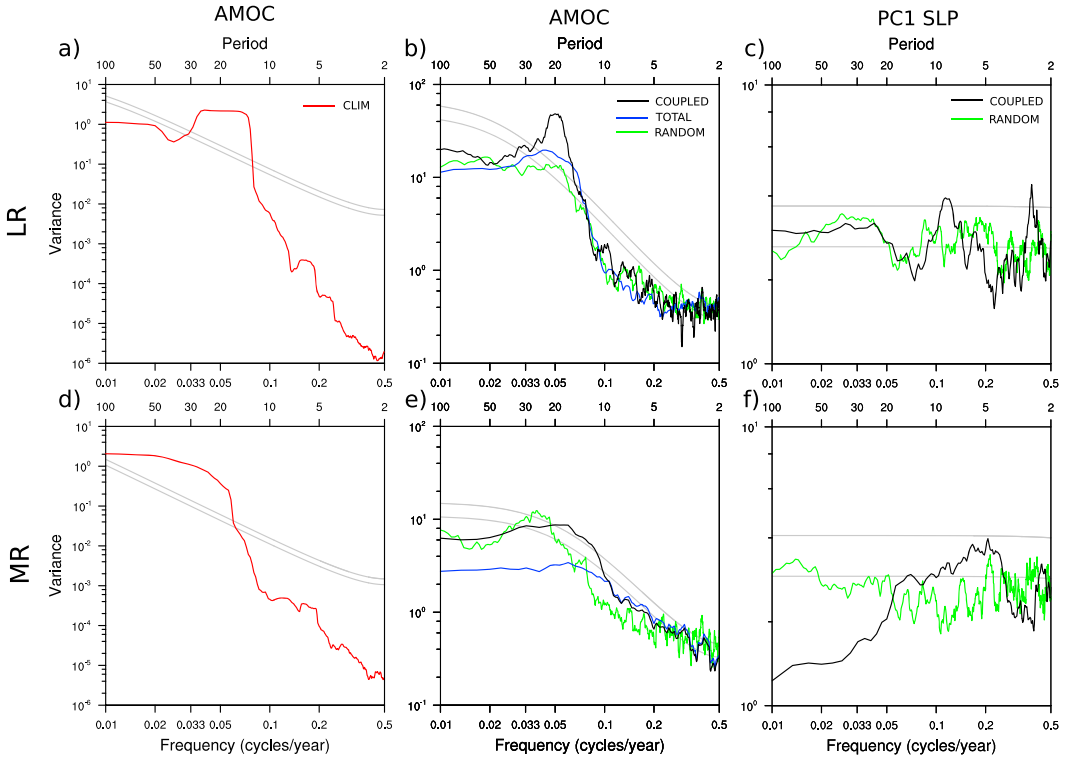

Figure 5. (a) Variance frequency spectrum of the AMOC index for CLIM-LR. (b) Same as (a) for (green) RANDOM-LR, (blue) ensemble mean of TOTAL-LR, and (black) COUPLED-LR simulation. (c) Variance frequency spectrum of the North Atlantic Oscillation index, defined as the PC1 of the SLP for (green) RANDOM-LR and (black) COUPLED-LR simulation. (d), (e), and (f) are the same as (a), (b), and (c) for the MR simulations. The spectra are calculated via fast Fourier transform. The theoretical Markov spectrum and the upper 95% confidence curve using the lag-1 autocorrelation are shown for the CLIM (panels a and d) or COUPLED (panels b, c, e, and f) simulations in gray lines. Note that the scale of the *y* axis is different in each column. AMOC = Atlantic Meridional Overturning Circulation; PC = principal component; SLP = sea level pressure. See Table 1 and section 2.2 for simulation name and experimental protocol.

without atmospheric stochastic forcing. It is the expression of the intrinsic oceanic variability. We first analyze the variability in CLIM-LR. After a relatively short transient adjustment period of about 50 years, the AMOC and AMV in the CLIM-LR simulation exhibit clear and regular decadal oscillations (Figure 2). The amplitude of the oscillation increases during the first 200 years of the experiment and decreases in the last 200 years, suggesting either a damped variability on a centennial time scale or sensitivity to a small mean state drift. The frequency content of the AMOC variability is further illustrated in Figure 5 in order to better characterize the self-sustained oceanic intrinsic variability. In CLIM-LR (Figure 5a, red line), the AMOC variance shows a clear maximum around 15 to 25 years, while a peak at 20 years is found in COUPLED-LR (Figure 5b, black line). The AMV in CLIM-LR has a very similar variability (Figure 2b). Its pattern (Figure 4g) has anomalies centered in the subpolar regions at 55°N with negligible tropical SST anomalies, so that the typical AMV horseshoe shape is not reproduced. The amplitude is 0.3 K for the maximum subpolar AMV SST anomalies, so that the subpolar AMV amplitude is reduced by 30% or 40% when compared to the fully coupled model.

As the atmospheric fluxes imposed in the CLIM-LR simulation have no interannual or decadal variability, the decadal variability obtained here can only be ascribed to an intrinsic oceanic mode. Using a similar experimental protocol, Delworth and Greatbatch (2000) analyzed the variability produced by the GFDL coupled model, which showed a pronounced variability for periods between 70 and 100 years. They found that such variability was not reproduced in their oceanic run using climatological flux forcing. It is likely that the oceanic mode detected here was more damped or not detected in the simulation of Delworth and Greatbatch (2000). The processes leading to this variability will be discussed in the following section.

The results based on the MR configuration are contrasting. The AMOC and AMV variability is much weaker in CLIM-MR after a 50-year adjustment period (Figure 2, dashed line). In CLIM-LM, the AMOC has enhanced

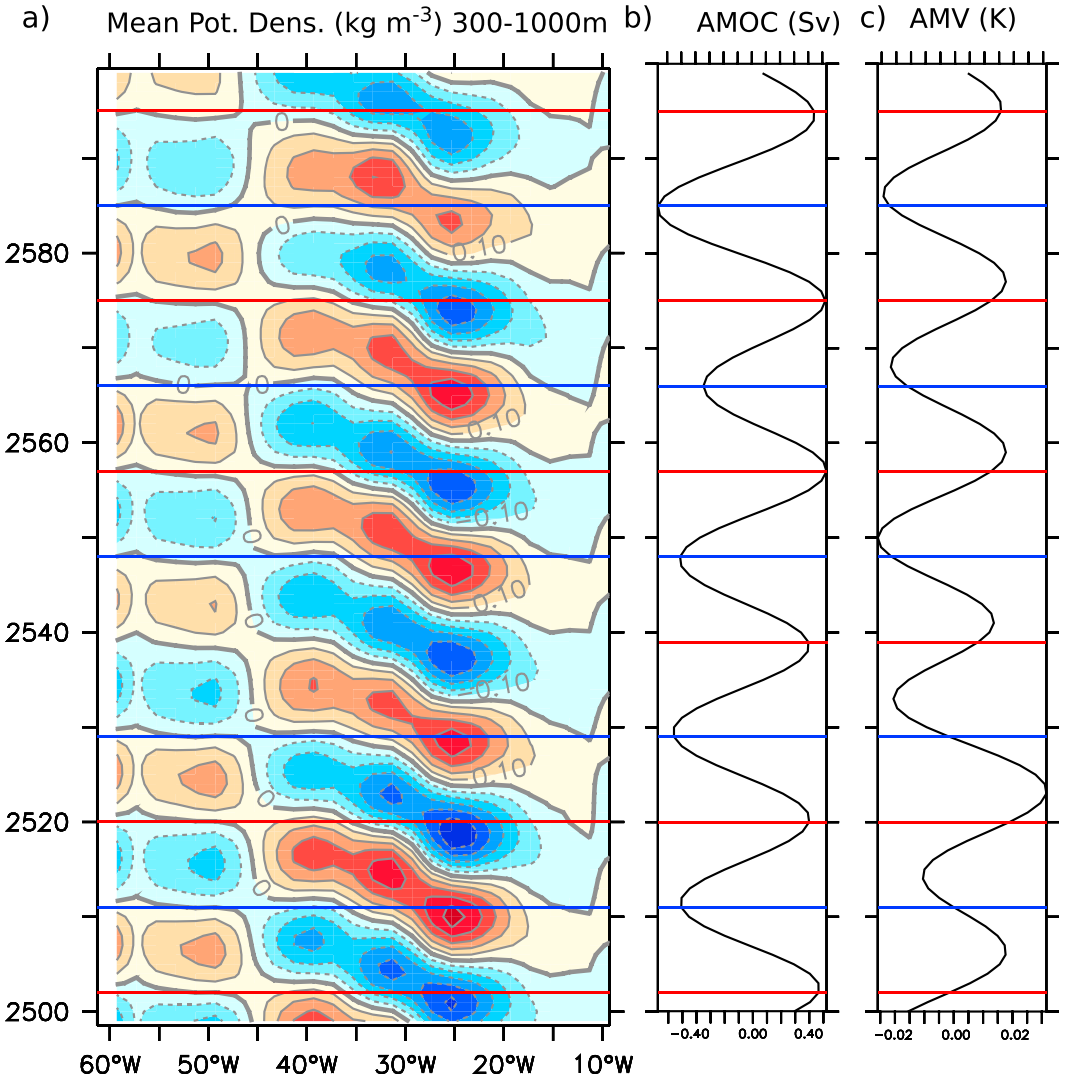

Figure 6. (a) Seawater density anomalies (kg/m^3) averaged in 50–60°N (region displayed in Figures 3g and 3h) for a period of 100 years of CLIM-LR. (b) AMOC anomalies (Sv), for the 100-year period of CLIM-LR corresponding to panel (a). (c) Same as (b) but for the AMV time series (K). The blue (red) line denotes the AMOC minimum (maximum). No smoothing was applied to the time series. AMOC = Atlantic Meridional Overturning Circulation; AMV = Atlantic multidecadal variability.

power for periods of 25 years and beyond (Figure 5d, red line), but no periodicity dominates at decadal time scales, with again levels of variability weaker than CLIM-LR (scale of *y* axis different in Figures 5a and 5d and Figures 5b and 5e). The AMV (Figure 4h) shows two bands of positive anomalies, at 45°N and 55°N in the Atlantic Ocean, with a maximum amplitude of 0.1 K. The ocean internal variability emerging from the subpolar regions in CLIM-LR is, therefore, likely to have a much weaker influence in CLIM-MR, and little internal oceanic mode is found when using the climatological forcing from the COUPLED-MR runs, as found in Delworth and Greatbatch (2000). The reasons for this different behavior in the MR and LR configuration will be discussed later.

3.2. Processes of Intrinsic Oceanic Variability in CLIM-LR

To illustrate the variability of the subpolar Atlantic basin found in CLIM-LR, the time evolution of the sea water density anomalies averaged between 0 and 700 m and between 50°N and 60°N in latitude (see dashed box in Figure 3, bottom) is shown in Figure 6a as a function of longitude. Anomalies appear around 25°W, at the east of the mid-Atlantic Ridge, in the west European basin, with a periodicity of about 20 years. They propagate from 25°W to 40°W in about 6 years, with a speed of about 0.5 cm/s. Then, they vanish at 45°W, at the

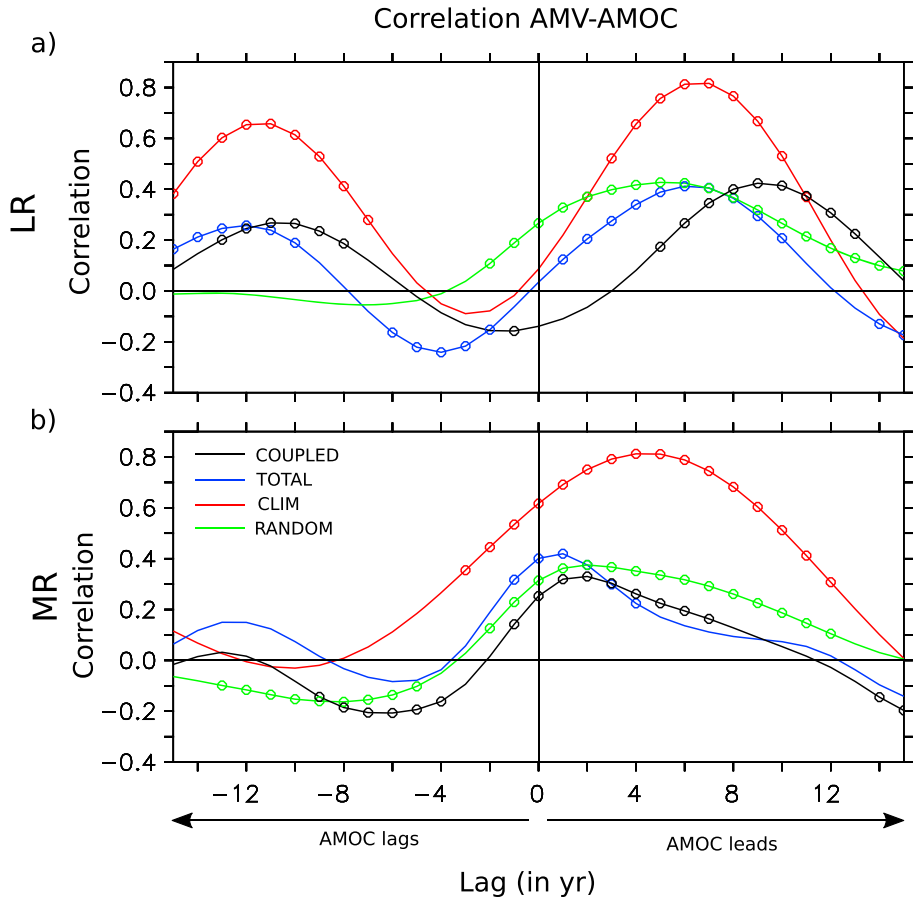

Figure 7. Lagged correlation between the AMOC and the AMV for (a) LR and (b) MR simulations. The lag (in year) is positive when the AMOC leads. The color is black for the COUPLED simulation, red for CLIM, blue for TOTAL, and green for RANDOM. The circles indicate level of significance below 5%. AMOC = Atlantic Meridional Overturning Circulation; AMV = Atlantic multidecadal variability. See Table 1 and section 2.2 for simulation name and experimental protocol.

southern tip of Greenland. The AMOC (Figure 6b) is maximum 1 or 2 years after formation of the negative density anomalies at 25°W. The subpolar north Atlantic basin is then marked by a large east-west density anomaly dipole which is associated with an anomalous northward current. The AMV maximum occurs 6 to 7 years after the maximum AMOC (Figures 6c and 7a, red line), which is consistent with a delayed impact of the intensified northward heat transport following the AMOC intensification.

The physics of the internal oceanic variability in CLIM-LR can be understood with previous studies based on the IPSL-CM5A-LR model (Ortega et al., 2015) or on the linear and adjoint version of the same ocean model (Sévellec & Fedorov, 2013). The characteristics of the mode include a westward propagation of unstable planetary waves at subpolar latitudes, a quarter phase lag between surface and subsurface temperature anomalies in the region of growth of perturbations, and a period of about 20 years. Large-scale baroclinic instability has been shown to be at the heart of the existence of such internal oceanic modes in idealized geometry (Colin de Verdière & Huck, 1999). In CLIM-LR, the region of growth for perturbations is located around 25°W, 55°N, at the southwestern edge of the deep water formation site, in the west European basin, as illustrated by the regression of the upper 700 m seawater density onto the AMOC (Figure 8a). The density anomalies are dominated by the temperature anomalies (Figure 8d). The regression of the density when AMOC is leading by 5 years (Figure 8b) illustrates that negative anomalies have propagated westward, consistently with Figure 6, while positive density anomalies dominated by the salinity appear at 50°N off Newfoundland (Figure 8e). Hence, the surface salinity anomalies in the Labrador Sea might act as a positive feedback for the oceanic variability, as they are advected by the mean surface current to the main region of

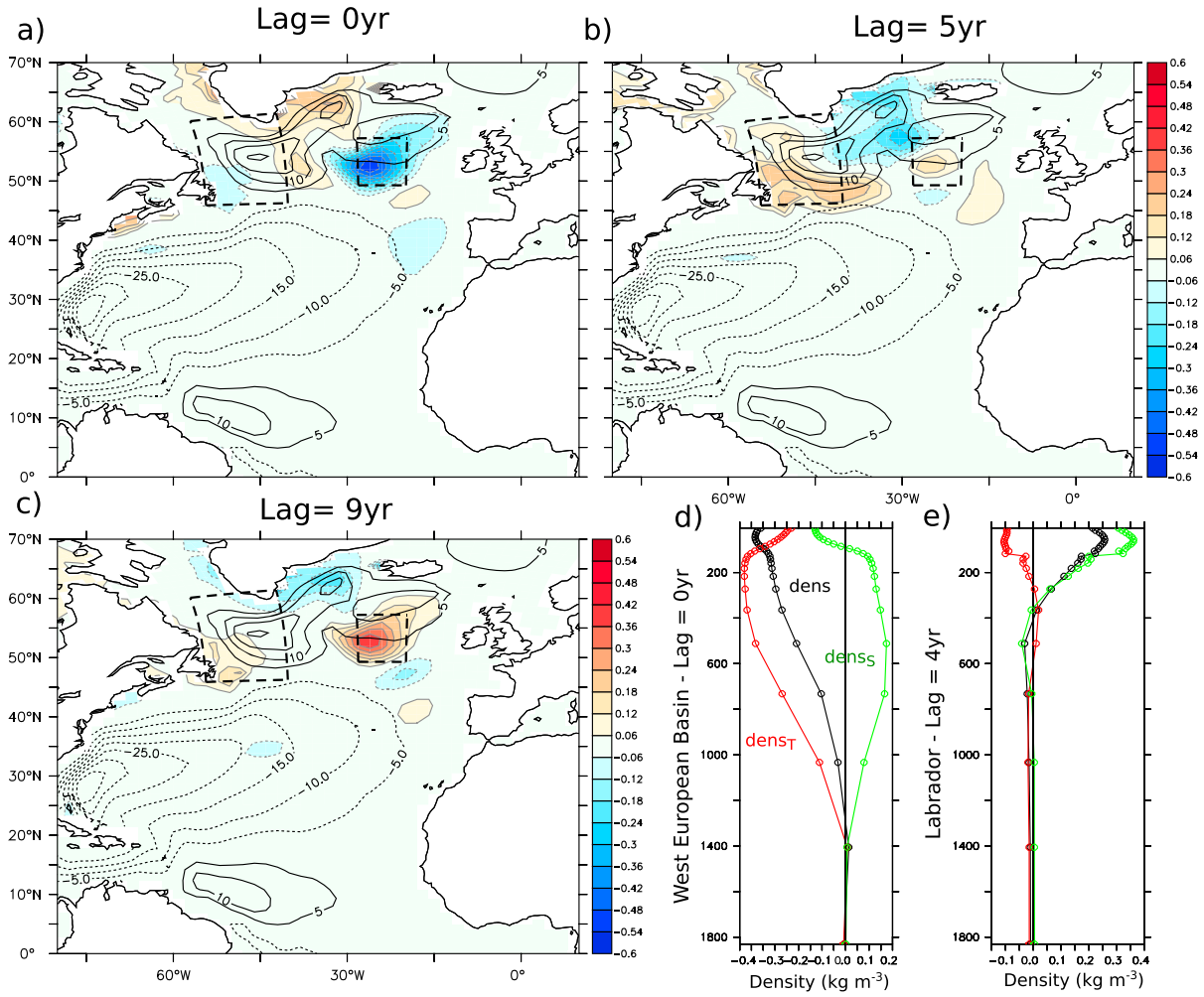

Figure 8. Regression of the 0- to 700-m density anomalies, (kg/m^3) onto the AMOC index in CLIM-LR, for (a) simultaneous fields (lag = 0 year) and when the AMOC leads by (b) 5 years and (c) 9 years. The thick black contours indicate the mean barotropic stream function (Sv). (d) Regression of density anomalies averaged over the west European basin with a lag of 0 year (region illustrated by dashed lines in panels a–c). The black line indicates the total density anomalies, the green line indicates the salinity-driven density anomalies, while the red line is the temperature-driven density anomaly. (e) Same as (d) but for the density anomalies averaged in the Labrador Sea entrance with a lag of 5 years (region illustrated by dashed lines in panels a–c).

deep water formation, as found in Escudier et al. (2013) or Ortega et al. (2015). The density lagging by 9 years shows a pattern opposite to that in phase with the AMOC (Figure 8c).

The process for the oceanic variability in CLIM-LR can be further investigated using the density variance budget, following Arzel et al. (2006), with the equation below:

$$\frac{1}{2}\frac{\partial\left\langle\overline{\rho'^2}\right\rangle}{\partial t} = -\left\langle\overline{\boldsymbol{u}}.\nabla\overline{\rho'^2}\right\rangle - \left\langle\overline{\boldsymbol{u}'\rho'}.\nabla\overline{\rho}\right\rangle + \left\langle\overline{\rho' B'}\right\rangle + \left\langle\overline{\rho' D'}\right\rangle \quad (1)$$

where ρ is the sea water density. The overbar and prime denote, respectively, time average over the whole simulation and deviation from the time average. The angle brackets denote depth average over the top 700 m. B' is the net anomalous density forcing calculated from the surface freshwater and heat flux integrated within the oceanic mixed layer, assuming a linear equation of state. D' is the density tendency due to the parameterized turbulent diffusion. $\boldsymbol{u}$ is the oceanic current. The first term on the right-hand side represents the advection of density variance by the mean flow. The second term is positive when eddy fluxes are oriented down the mean density gradient and was previously associated with baroclinic instabilities (Colin de Verdière & Huck, 1999). The third term is associated with the surface boundary conditions: Positive

values indicate that air-sea interactions increase the density variance and contribute thereby to the development of the variability, while negative ones imply a damping of the variability by air-sea coupling. The last term represents the dissipation of variance by convective mixing and turbulent eddy diffusion and is always negative.

The different terms of the density variance budget computed from yearly outputs are shown in Figure 9 (shading, left column) for CLIM-LR, together with the mean current averaged over 0–300 m (vectors). Most of the growth of density variance is caused by the action of the eddy fluxes (Figure 9c) in the west European basin, at 30°W, 52°N, and in the Irminger Sea. Such density flux in the west European basin is dominated the meridional component and are mainly due to temperature-driven density anomalies (not shown), as found in Figure 8d. The advection of the density variance (Figure 9e) transports the variance downstream of the mean currents while surface buoyancy fluxes (Figure 9g) are weak and act as a damping. This analysis strongly suggests that the existence of low-frequency variability in CLIM-LR is due to a (large-scale) baroclinic instability of the mean flow in the west European basin. This conclusion is supported by the vertical structure of the temperature anomalies between 100 and 1,500 m (see supporting information Figure S2) that exhibits a phase lag of about a quarter period, with the surface anomalies leading the deeper ones, in agreement with the organization of perturbations in a zonal shear flow under quasi-geostrophic dynamics. We did not find any major sources of density variability in the Labrador Sea, where the salinity-driven density anomalies are found in Figure 8e.

3.3. Processes of Intrinsic Oceanic Variability in CLIM-MR

A similar analysis was performed in CLIM-MR. In this configuration, the density anomalies averaged in 0–700 m and 50–60°N are weaker and the propagation is less periodic (not shown). The AMV has a positive correlation with the AMOC in this simulation, with a maximum when the AMOC leads by 5 years (Figure 7b), consistent with the results of CLIM-LR.

The AMOC is also correlated with the density anomalies at 50°N, 30°W in CLIM-MR. The pattern is somehow similar to that shown in Figure 8, but the values are divided by 5 in amplitude and we did not detect any density anomalies west of 40°W (not shown). The density variance budget for CLIM-MR (Figure 9, right column) shows that an important eddy flux (Figure 9d) does generate some density variance in the west European basin, especially at 52°N, 30°W, at 56°N, 30°W, and North of Iceland, but those instabilities are small (see different scale for left and right columns in Figure 9). The dominant eddy flux terms are at the same location as CLIM-LR, which emphasizes the importance of baroclinic instability at this location. The density variance is then advected by the mean flow (Figure 9f), while the surface boundary conditions damp the variability (Figure 9h).

In summary, CLIM-MR shows some very weak decadal variability with characteristics similar to that of CLIM-LR. We will see next that the mean state difference caused by the different atmospheric resolution leads to a strong damping of the oceanic intrinsic mode.

3.4. Role of Atmospheric Resolution

As discussed previously, the Atlantic Ocean decadal variability of CLIM-LR is much stronger than in CLIM-MR, which is consistent with the results from the corresponding coupled models. This difference may be traced back to the small differences in the climatological fields forcing the ocean. Indeed, the atmospheric resolution in the IPSL-CM5A model has an impact on the latitudinal position of the midlatitude westerlies (Arakelian & Codron, 2012). Consequently, COUPLED-MR simulates stronger westerly wind stress between 50°N and 60°N, as the southward bias of the eddy driven jets in COUPLED-LR is reduced in COUPLED-MR with enhanced resolution (Dufresne et al., 2013). The mean SLP in MR (Figure 10a) also shows a stronger Icelandic low. This might be explained by the different tuning of the atmospheric radiative budget, subgrid scale orographic parametrization, or horizontal dissipation. The more intense Icelandic low in COUPLED-MR induces stronger cold air advection over the western part of the subpolar gyre, thereby leading to more intense surface cooling (Figure 10a) and positive density anomalies over that region (Figures 10c and 10d) as compared to COUPLED-LR. Consequently, the subpolar gyre is more intense in the western Atlantic, particularly around 35°W, 50°N, while it contracts and weakens in the eastern Atlantic and south of Iceland (Figures 10c and 10d). This warms the west European basin and increases the stratification, which may contribute to inhibit the instability growth together with the modified oceanic current. This also modifies

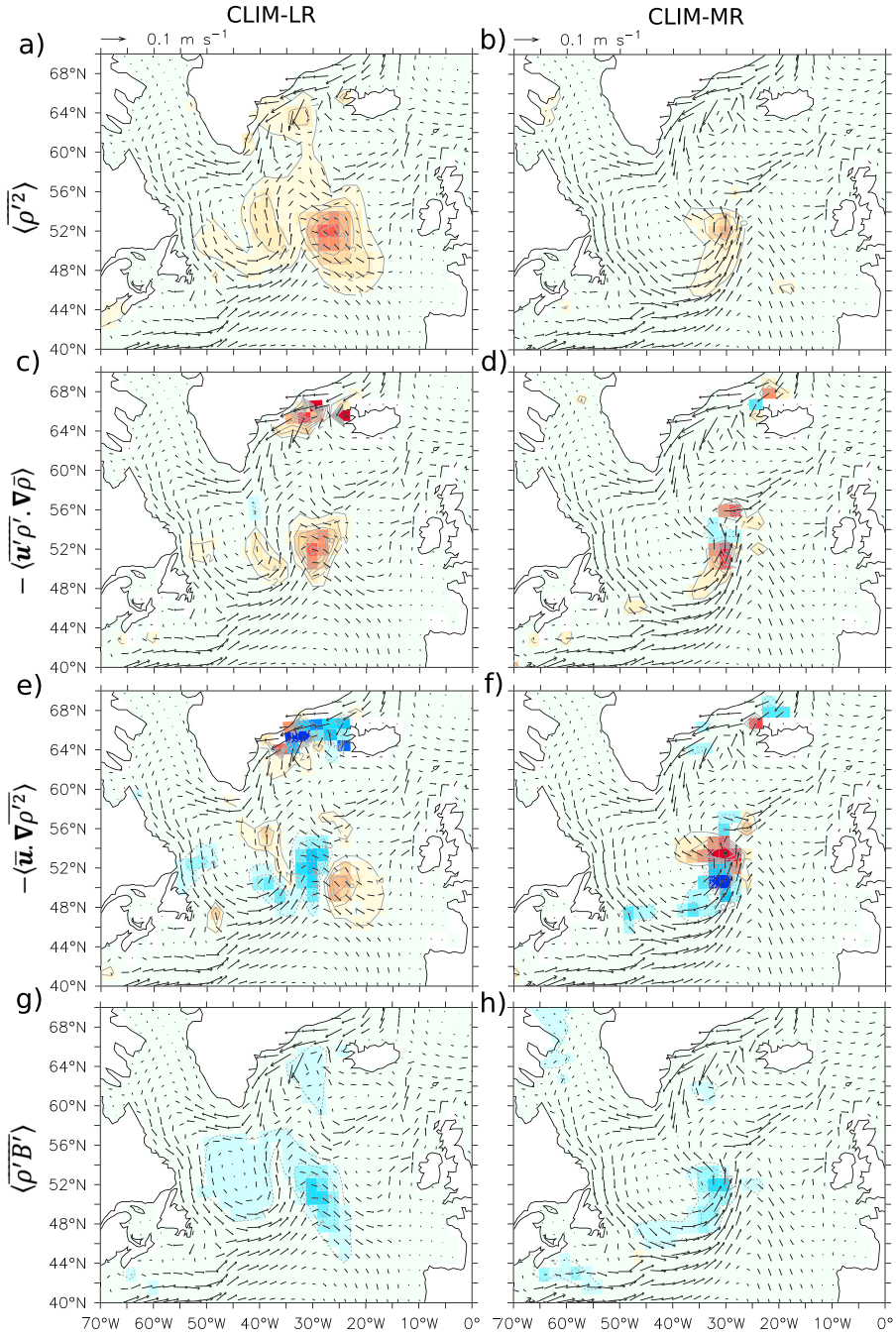

Figure 9. Mean density interannual variance, at 0- to 700-m depth (color shadings; $(kg/m^3)^2$), in (a) CLIM-LR and (b) CLIM-MR. Density variance tendency, in 10^{-3} $(kg\ m^{-3})^2\ yr^{-1}$, induced by the eddy density transport down the zonal density gradient, in (c) CLIM-LR and (d) CLIM-MR. (e) and (f) are the same as (c) and (d) but for the mean advection of density variance. Density variance tendency, in 10^{-4} $(kg\ m^{-3})^2\ yr^{-1}$, induced by the surface buoyancy forcing, in (g) CLIM-LR and (h) CLIM-MR. In all panels, the vectors illustrate the mean oceanic current in the top 300 m. Note the difference in contour interval for CLIM-LR and CLIM-LR and in panels (a–f) and (g–h). See Table 1 and section 2.2 for simulation name and experimental protocol.

in MR the water transport into the convection sites located South of Iceland (blue dotted contours in Figures 10c and 10d), which ultimately reduces the deep water formation South of Iceland and increases it further west, in the center of the subpolar gyre (Figure 10b). Such a link between the subpolar gyre extent and deep convection areas has been reported in several previous studies (Häkkinen & Rhines, 2004; Hátún

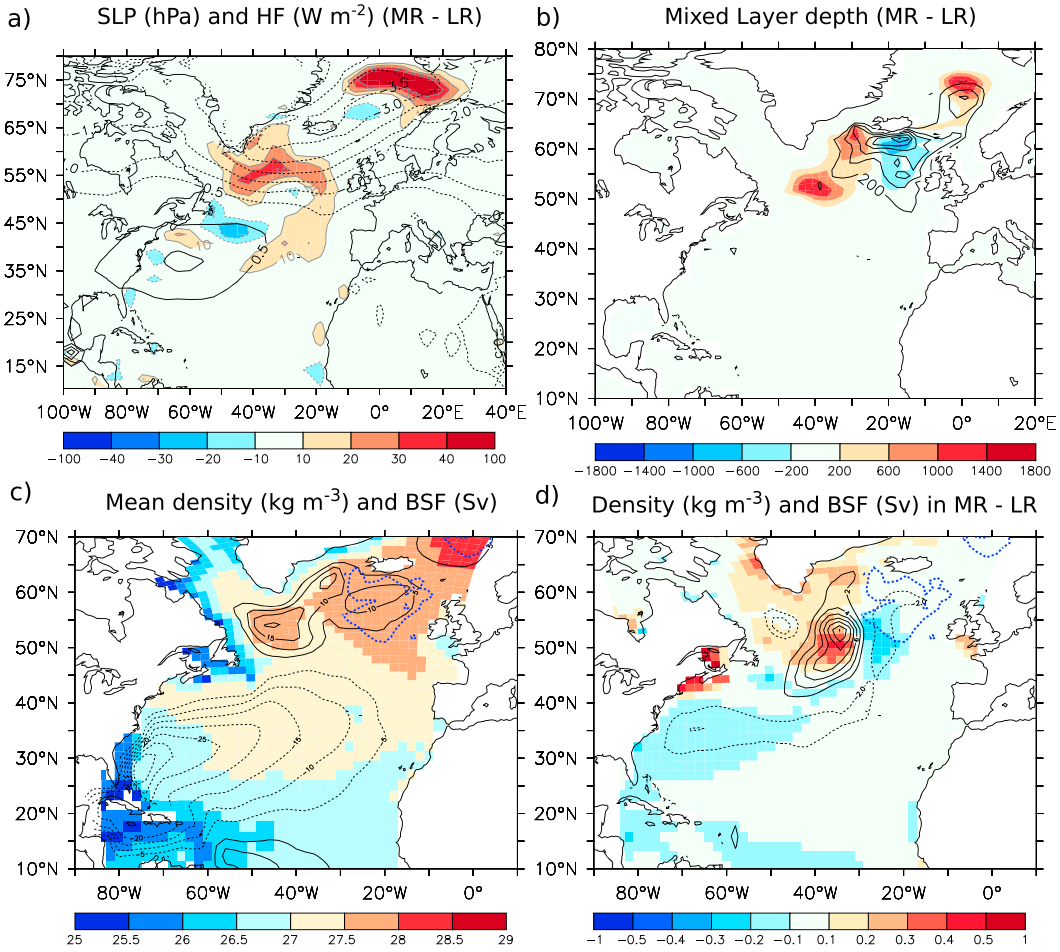

Figure 10. (a) Mean surface heat flux (color, positive upward; W/m^2), and (black contours) SLP (hPa), difference between COUPLED-MR and COUPLED-LR simulation. (b) Mean February-March-April (FMA) mixed layer depth difference (color; m), between COUPLED-MR and COUPLED-LR simulation, and (black contours) mean FMA mixed layer depth in COUPLED-LR. (c) Mean subsurface potential density (color; kg/m^3) for the upper 300 m in CLIM-LR, and (black contours) mean barotropic stream function (Sv). (d) Same as (c) but for the difference of the CLIM-MR and CLIM-LR. The thick blue dash contour in panels (c and d) indicates the difference in the yearly mixed layer depth standard deviation (contour interval 25 m). SLP = sea level pressure. See Table 1 and section 2.2 for simulation name and experimental protocol.

et al., 2005; Langehaug et al., 2012). However, these studies involve the Nordic seas rather than the convection site South of Iceland as here. The lack of penetration of the oceanic circulation into the Nordic Seas is a bias of this model with both atmospheric resolutions.

4. Role of the Atmospheric Stochastic Forcing and Coupling for the AMOC Variability

4.1. Role of Atmospheric Stochastic Forcing

The surface boundary conditions used in the RANDOM simulations do include some variability beyond the seasonal cycle. That was not the case for the CLIM simulations using a repeated identical seasonal cycle. In this section, the results from RANDOM are analyzed and compared to CLIM to illustrate the role of the atmospheric stochastic forcing.

We first evaluate the atmospheric variability imposed to the ocean in the RANDOM simulations. We characterize the atmospheric variability by the leading empirical orthogonal functions of the North Atlantic SLP (see section 2.3 for details). The NAO patterns (see supporting information Figure S3) are similar for LR and MR, but the NAO has more intense centers of action in LR, with an anomaly of the Acores high of 4.3 hPa (3.8 hPa) and an Icelandic low anomaly of −4.7 hPa (4.2 hPa) in LR (MR). This is consistent with a

larger SLP variance over most of the Atlantic Ocean in LR (see supporting information Figure S4). Figures 5c and 5d (green lines) show the spectra of the NAO associated with the surface boundary conditions of the RANDOM simulations. The spectra are similar to a white noise spectrum in both the LR and MR cases, which illustrates that the random permutations have led to generate a stochastic atmospheric forcing consistent with the one of a white noise. In summary, the amplitude of the atmospheric stochastic forcing is larger in LR than in MR. Moreover, no periodicity emerges in the spectrum of the forcing applied in RANDOM.

The AMOC resulting from the variable surface boundary condition in RANDOM experiences a much larger variability than in CLIM, from interannual to interdecadal time scales, irrespective of the atmospheric resolution (Table 1). The variance of the 0–700 m North Atlantic potential temperature (Figures 3e and 3f) is also much larger in RANDOM when compared to CLIM, with a ratio among standard deviations of about 5 in both LR and MR configurations. Nevertheless, both the AMOC and North Atlantic subsurface temperature variability are larger in RANDOM-LR than in RANDOM-MR, which is consistent with the larger atmospheric stochastic forcing in LR. The AMV pattern in RANDOM (Figures 4e and 4f) has the typical comma shape with SST anomalies maximum in the subpolar Atlantic and weaker anomalies in the east of the subtropical Atlantic gyre. The maximum AMV anomalies in RANDOM-LR (+0.4 K) are located south of the Irminger basin, which coincides with that obtained in CLIM-LR (+0.3 K) with slightly larger amplitude. The maximum anomalies for RANDOM-MR (+0.3 K) are located in the center of the Atlantic Ocean at 45°N, farther east of the maximum anomalies found in CLIM-MR (+0.1 K) with much a larger amplitude. Again, the AMV anomalies are weaker in RANDOM-MR than in RANDOM-LR as the atmospheric forcing is weaker. In both LR and MR, the AMV pattern of RANDOM has many of the AMV characteristics produced by TOTAL, in terms of amplitude or latitudinal extension. This confirms the dominant role of atmospheric stochastic forcing for the AMV characteristics, through the time integration of the atmospheric noise within the oceanic mixed layer (Cane et al., 2017; Clement et al., 2015) or through the excitation of the internal mode described previously.

The lag between the AMV and the AMOC is 5 years in RANDOM-LR and 2 years in RANDOM-MR (Figure 7, green line), which is shorter than the lag obtained in the CLIM simulations. The correlation between the AMV and the AMOC is also smaller, but it remains significant at the 5% level. We can conclude that including a stochastic forcing may reduce the AMV-AMOC relationship and alter the time lag between the ocean and the atmosphere.

Lastly, we illustrate the lagged correlation between the AMOC and NAO in Figure 11. In RANDOM-LR (green curve in Figure 11a), the NAO is negatively correlated with the AMOC at lag 0, but it also has a marginal but significant correlation when the positive NAO leads the AMOC by 2 years. In RANDOM-MR (Figure 11b), the links are similar, but the simultaneous relationships are larger, and the NAO has also a larger lagged influence onto the AMOC than in the LR, detected from lag −1 years to lag −11 years. It agrees with the influence of the NAO onto the AMOC (Eden & Willebrand, 2001; Gastineau & Frankignoul, 2012; Mignot & Frankignoul, 2005): The NAO causes a fast barotropic response through Ekman currents in phase and a delayed more persistent baroclinic response. This also shows that the delayed NAO stochastic forcing has more impact in the MR configuration than in the LR one. This reflects the lower levels of internal oceanic decadal variability found in MR and relatively more important atmospheric stochastic forcing processes for the AMOC.

4.2. Role of Coupling: The LR Case

We have shown in section 2.4 that TOTAL-LR simulates a decadal variability comparable to that of the COUPLED-LR simulations in terms of AMOC (Figure 1), subsurface temperature (Figure 3), or AMV (Figure 4) variability, even if the use of surface restoring leads to weaker SST anomalies. Figure 5 further illustrates that the decadal variability is weaker in TOTAL-LR when compared to COUPLED-LR; however, a maximum variance between 15 and 20 years is still present for TOTAL-LR.

The role of air-sea coupling is inferred by comparing the RANDOM and TOTAL simulations. The forcing used in TOTAL includes both an atmospheric stochastic forcing and the atmospheric response to the ocean as simulated in COUPLED. This forcing may therefore include some decadal variability that may in turn modify the oceanic decadal variability. Conversely, the forcing in RANDOM is built so that the decadal variability is randomized. The forcing used in RANDOM and the oceanic variability are, therefore, uncorrelated at decadal time scale. We first focus on the LR simulations. The simulation TOTAL-LR (Figure 5b, blue line) shows a more important variance at 15–25 years, when compared to RANDOM-LR (Figure 5b, green line). The patterns of the 0–700 m potential temperature standard deviation (Figure 3) or the AMV (Figure 4) have a large

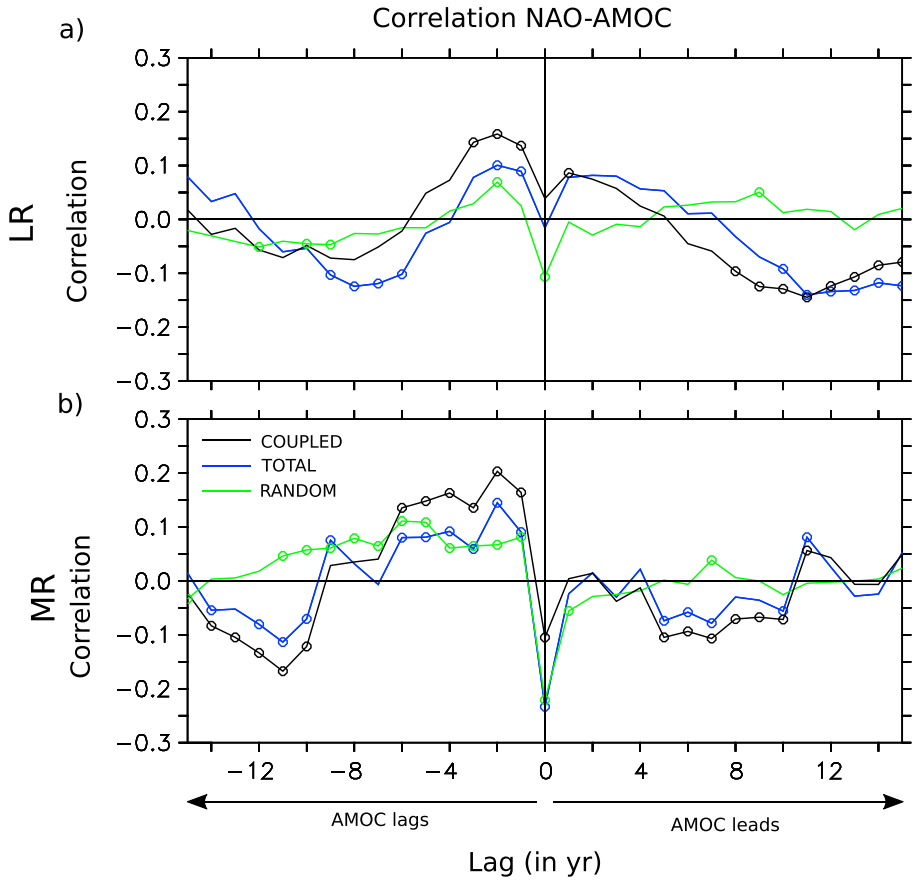

Figure 11. Cross-correlation between the AMOC and the NAO indices in (a) LR and (b) MR simulations. The lag (year) is positive when the AMOC leads. The color is black for the COUPLED simulation, blue for TOTAL, and green for RANDOM. The circles indicate level of significance below 5%. AMOC = Atlantic Meridional Overturning Circulation; NAO = North Atlantic Oscillation. See Table 1 and section 2.2 for simulation name and experimental protocol.

degree of similarity, which confirms the dominant role of atmospheric stochastic forcing, in both TOTAL-LR and RANDOM-LR. The lag between the AMOC and the AMV is also similar in both simulations (Figure 7a). However, the AMV pattern shows larger anomalies at 40°N east of 40°W in RANDOM, so that the decadal variability of the SST is different in the two simulations. This can be explained by the weaker negative surface heat flux feedback in RANDOM, as the heat flux does not always act to damp the SST anomalies in this simulation.

We calculate the passband variance of the subpolar subsurface (0–700 m) potential temperature and AMOC, using 10–30 years as passband periods (Table 1). The analysis reveals that the decadal variability in both the subpolar heat content and the AMOC are larger in TOTAL than in RANDOM. This difference is significant at the 5% level only when using a passband filtered AMOC index. We conclude that air-sea coupling increases the amplitude of the intrinsic decadal variability. The passband (10–30 years) filtered AMOC standard deviation is further investigated in Figure 12, illustrating that the amplification of the meridional overturning stream function variability is not restricted to the subpolar region and is simulated over the whole Atlantic basin.

The interplay between AMOC changes and the NAO can be inferred by computing the lag correlation between those two indices (Figure 11, black line). The analysis shows that the NAO reaches a negative phase 8 to 15 years after an AMOC maximum in TOTAL-LR. This relationship is consistent with the results of COUPLED-LR and previous studies (Gastineau et al., 2013; Gastineau et al., 2016): The SST associated with the AMOC causes a negative NAO atmospheric response when the AMOC leads by 8 to 15 years. As the AMOC has a dominant ~20-year periodicity, this negative NAO response that follows by 8 to 15 years an AMOC intensification occurs during an AMOC minimum. Such negative NAO pattern causes a weakening

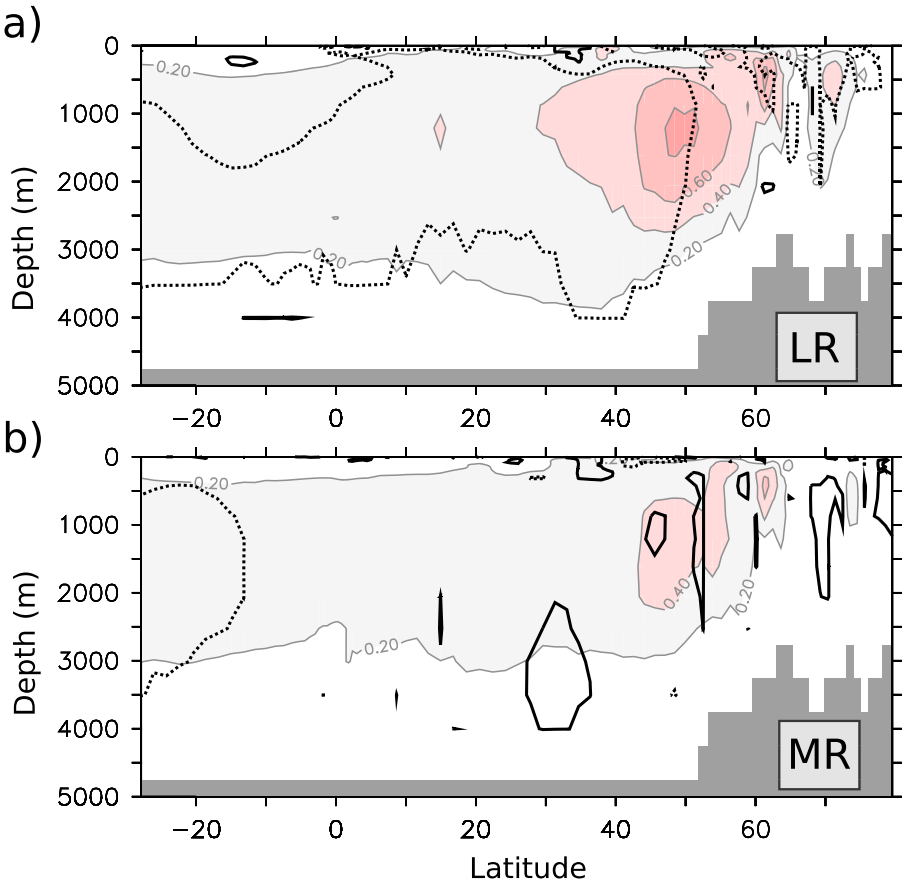

Figure 12. (a) Standard deviation of the yearly band-pass (10 and 30 years) filtered Atlantic meridional stream function (Sv), for TOTAL-LR (shading). The thick black lines indicate where the variance for the yearly band-pass (10 and 30 years) filtered stream function is lower (full line) or larger (dashed line) in RANDOM-LR when compared to TOTAL-LR, with a *p* value lower than 5%. (b) Same as (a) but for the MR simulations. See Table 1 and section 2.2 for simulation name and experimental protocol.

of the AMOC (Eden & Willebrand, 2001; Gastineau & Frankignoul, 2012; Mignot & Frankignoul, 2005), which may reinforce the AMOC minimum. Therefore, we speculate that the negative NAO response to an intense AMOC in LR explains the intensification of the 20-year oceanic variability.

4.3. Role of Coupling: The MR Case

We now compare TOTAL-MR and RANDOM-MR to see the effect of coupling in the case of the MR simulations. Again, the standard deviation of the 0–700 m potential temperature or the AMV patterns are roughly similar, even if the amplitudes are slightly larger in RANDOM-MR than in TOTAL-MR. The lagged correlation between the AMOC and the AMV are comparable in both simulations (Figure 7b). The AMOC of RANDOM-MR has more variance than TOTAL-MR in particular for periods larger than 15 years (Figure 5e). This is consistent the larger NAO variance in RANDOM-MR at these periods (see Figure 5e). In Table 1, the variance of the yearly AMOC and subsurface subpolar temperature also show larger values in RANDOM when compared to TOTAL. However, when using the passband variance at 10–30 years, we do not detect any significant changes in the AMOC variance at the 5% level. This is consistent with Figure 12b, where the variance of the AMOC is found to increase, although this increase is not statistically significant at the 5% level.

Lastly, a negative correlation between NAO and AMOC is found in TOTAL-MR when the AMOC leads by 5 to 10 years (see Figure 11b). The atmospheric response is expected to act as a positive feedback for the oceanic variability, as found in the LR case. However, the periodicity of the AMOC variability in MR is different from that of LR, with more variance at periods larger than 20 years, so that this positive feedback is not detected here.

In summary, the coupling leads to a weak damping of the multidecadal AMOC variability in the MR case. As the oceanic internal variability is weak in MR, it is likely that the coupling does not influence it. This difference obtained probably reflects the different atmospheric stochastic forcing in RANDOM-MR and TOTAL-MR, as the NAO of RANDOM-MR has more power at multidecadal frequencies (Figure 5f).

5. Discussion and Conclusions

We have investigated the processes of the decadal variability in the coupled climate models IPSL-CM5A-LR (called COUPLED-LR) and IPSL-CM5A-MR (called COUPLED-MR). In COUPLED-LR, the Atlantic subpolar basin exhibits a clear intrinsic decadal variability with a 20-year period. The variability is dominant when climatological forcing (repeated seasonal cycle) derived from the coupled simulation is applied to an ocean-only simulation. The variability is associated with westward propagating density anomalies at 55°N in the eastern subpolar basin, similar to Sévellec and Fedorov (2013). The density variance budget reveals the central role of transient temperature fluxes in extracting potential energy from the mean flow to grow perturbations. This suggests that the decadal variability in the model is caused by a large-scale baroclinic instability of the mean flow at subpolar latitudes. In addition to this mechanism, we verified that the subpolar density anomalies appear to be influenced by waters originating from the East Greenland Current. Ortega et al. (2015) showed with the control simulation of IPSL-CM5A-LR (identical to COUPLED-LR in the present study) that the East Greenland Current leads to large salinity-dominated density anomalies in the Labrador Sea entrance, that are then advected by the mean current, acting as a positive feedback for the North Atlantic decadal variability. Although we did not specifically investigate this process here, we detected some salinity-driven density anomalies in the Labrador Sea, so that it is likely that the same process is also playing a role in the simulation investigated here.

We found that the MR model configuration is consistently generating less decadal variability in coupled and ocean-only climatologically forced conditions. In the MR simulation, the AMOC is more intense with warmer mean temperature and less sea ice extent. The Icelandic low is also deeper, and the westerlies are stronger over the subpolar gyre. This leads to different momentum and heat air-sea exchanges acting to intensify the subpolar gyre west of the mid-Atlantic Ridge and to decrease it east of the ridge. The North Atlantic current is more zonal and intense, bringing more warm water at surface to the west European basin where the density anomalies are generated. Both the stronger stratification of the seawater in the top 700 m and the different oceanic currents in the west European basin may explain the lower oceanic internal variability in MR. A detailed stability analysis of the oceanic state would be needed to address this issue and is left for future work.

We did specific experiments to study the effect of atmospheric stochastic forcing and that of ocean-atmosphere coupling. The atmospheric stochastic forcing strongly amplifies the Atlantic decadal variability irrespective of the model version. However, the NAO amplitude is larger in LR than in MR, which is consistent with a larger impact of atmospheric forcing for the AMV and the AMOC variability in LR. In the case of LR, we evaluate that a significant part of the North Atlantic climate variability is associated with a self-sustained intrinsic oceanic mode: The standard deviation of the subpolar temperature in CLIM-LR is 19% that of RANDOM-LR, while that of the AMOC at 10–30 years in CLIM-LR is 44% that of RANDOM-LR (see Table 1). The coupling has a modest but significant impact in COUPLED-LR, as it intensifies the AMOC variability by 23% at periods of 10–30 years (see RANDOM-LR and TOTAL-LR in Table 1). In MR, the AMOC variability at 10–30 years is weaker and hardly modified by coupling. Such weak variability is consistent with the lower internal oceanic variability and the weaker atmospheric stochastic forcing. In the MR case, the randomization of the atmospheric forcing leads to slightly more variance at periods larger than 25 years, which enhances the AMOC multidecadal variability when using randomized atmospheric fluxes as surface boundary conditions.

In LR, the influence of air-sea coupling is consistent with a NAO response to the AMOC anomalies, acting to enhance the internal oceanic variability. Our results could appear paradoxical when compared to the study of Wen et al. (2016), where the interplay between the NAO and the AMOC was found to produce a strong positive feedback in COUPLED-MR. However, the focus in the present study is on the decadal AMOC variability, while the important simultaneous NAO-AMOC feedbacks described by Wen et al. (2016) are mainly relevant at interannual and shorter time scales.

We have also investigated specifically the AMV pattern produced by the oceanic internal variability and by the atmospheric stochastic forcing. We found that, although the atmospheric forcing is responsible for the typical AMV latitudinal extension and the characteristic comma shape (as in Clement et al., 2015), significant anomalies can be produced locally by the oceanic internal variability in the subpolar gyre. For instance, the averaged AMV anomaly (corresponding to one standard deviation of the AMV index) at 50–20°W, 48–60°N is 0.15 K in CLIM-LR, while it is equal to 0.22 K in RANDOM-LR, so that up to 68% of the AMV anomalies can be produced by the oceanic internal variability in the subpolar gyre, where the AMV SST anomalies are largest. Nevertheless, additional work would be needed to investigate the processes linking the atmospheric stochastic forcing and the AMV. Indeed, the AMV can be produced by the integration of the atmospheric noise within the oceanic mixed layer through thermodynamical processes (Clement et al., 2015; Frankignoul & Hasselmann, 1977) or by the amplification of the oceanic internal variability by atmospheric noise.

The variability generated in the IPSL-CM5A models is reproduced in the ocean-only simulations using climatological sea ice concentration with a simple representation for the air-sea exchanges at the ocean-ice interface. Such oceanic variability is therefore not sensitive to the accurate representation of the sea ice processes. Nevertheless, the experimental protocol could be repeated using the sea ice model from the COUPLED simulation, to reduce the mean state difference between the coupled and ocean-only simulation (see Figure 1). This would allow investigating the multidecadal variability emerging from the North Atlantic-Arctic exchanges (i.e., Frankcombe & Dijkstra, 2011; Jungclaus et al., 2005).

The experimental protocol used here could be repeated using more realistic fluxes based on observations to reveal the influence of model biases onto the decadal variability (Menary et al., 2015), in particular over the subpolar gyre region. The same methodology could also be used to understand the influence of the increasing greenhouse gases concentration, which may decrease the intensity of the AMOC and lead to a subpolar gyre cooling (Drijfhout et al., 2012; Rahmstorf et al., 2015). However, the simulations we have analyzed here use a low horizontal resolution ocean model and do not include mesoscale or submesoscale eddies that also generate important levels of intrinsic oceanic variability in models using higher horizontal resolution (Grégorio et al., 2015). We are currently interested in whether the large-scale baroclinic instability found here can occur with increasing horizontal resolution.

Lastly, these results also have interesting implications for the role of the mean state for the decadal variability. We found that relatively small changes in the mean stratification and circulation of the Atlantic subpolar gyre, as obtained when comparing CLIM-LR with CLIM-MR, lead to different levels of North Atlantic decadal variability. It is therefore crucial to reduce the mean bias of coupled models in the subpolar region to increase the realism of the simulated Atlantic decadal variability.

Acknowledgments
The access to the model data used in this study is listed in the supporting information. This research was supported by the French CNRS/INSU/LEFE-AO project MesoVarClim (PI: O. Arzel). This work was granted access to the HPC resources of TGCC under the allocations 2016-017403, 2017-017403, and A0030107403 made by GENCI. This study benefited from the IPSL mesocenter facility which is supported by CNRS, UPMC, and Labex L-IPSL, which is funded by the ANR (grant ANR-10-LABX-0018) and by the European FP7 IS-ENES2 project (grant 312979).

References

Arakelian, A., & Codron, F. (2012). Southern Hemisphere jet variability in the IPSL GCM at varying resolutions. *Journal of the Atmospheric Sciences*, *69*(12), 3788–3799. https://doi.org/10.1175/JAS-D-12-0119.1

Arzel, O., Huck, T., & Colin de Verdière, A. (2006). The different nature of the interdecadal variability of the thermohaline circulation under mixed and flux boundary conditions. *Journal of Physical Oceanography*, *36*(9), 1703–1718. https://doi.org/10.1175/JPO2938.1

Arzel, O., Huck, T., & Colin de Verdière, A. (2018). The internal generation of the Atlantic Ocean interdecadal variability. *Jornal of Climate*, *31*(16), 6411–6432. https://doi.org/10.1175/JCLI-D-17-0884.1

Bellucci, A., Gualdi, S., Scoccimarro, E., & Navarra, A. (2008). NAO–ocean circulation interactions in a coupled general circulation model. *Climate Dynamics*, *31*(7–8), 759–777. https://doi.org/10.1007/s00382-008-0408-4

Bretherton, C. S., Widmann, M., Dymnikov, V. P., Wallace, J. M., & Bladé, I. (1999). The effective number of spatial degrees of freedom of a time-varying field. *Journal of Climate*, *12*(7), 1990–2009. https://doi.org/10.1175/1520-0442(1999)012<1990:TENOSD>2.0.CO;2

Cane, M. A., Clement, A. C., Murphy, L. N., & Bellomo, K. (2017). Low-pass filtering, heat flux, and Atlantic multidecadal variability. *Journal of Climate*, *30*(18), 7529–7553. https://doi.org/10.1175/JCLI-D-16-0810.1

Cattiaux, J., Quesada, B., Arakélian, A., Codron, F., Vautard, R., & Yiou, P. (2013). North-Atlantic dynamics and European temperature extremes in the IPSL model: Sensitivity to atmospheric resolution. *Climate Dynamics*, *40*(9–10), 2293–2310. https://doi.org/10.1007/s00382-012-1529-3

Chylek, P., Folland, C. K., Dijkstra, H. A., Lesins, G., & Dubey, M. K. (2011). Ice-core data evidence for a prominent near 20 year time-scale of the Atlantic Multidecadal Oscillation. *Geophysical Research Letters*, *38*, L13704. https://doi.org/10.1029/2011GL047501

Clark, P. U., Pisias, N. G., Stocker, T. F., & Weaver, A. J. (2002). The role of the thermohaline circulation in abrupt climate change. *Nature*, *415*(6874), 863–869. https://doi.org/10.1038/415863a

Clement, A., Bellomo, K., Murphy, L. N., Cane, M. A., Mauritsen, T., Rädel, G., & Stevens, B. (2015). The Atlantic Multidecadal Oscillation without a role for ocean circulation. *Science*, *350*(6258), 320–324. https://doi.org/10.1126/science.aab3980

Colin de Verdière, A., & Huck, T. (1999). Baroclinic instability: An oceanic wavemaker for interdecadal variability. *Journal of Physical Oceanography*, *29*(5), 893–910. https://doi.org/10.1175/1520-0485(1999)029<0893:BIAOWF>2.0.CO;2

Danabasoglu, G., Yeager, S. G., Bailey, D., Behrens, E., Bentsen, M., Bi, D., et al. (2014). North Atlantic simulations in coordinated ocean-ice reference experiments phase II (CORE-II). Part I: Mean states. *Ocean Modelling*, *73*, 76–107. https://doi.org/10.1016/j.ocemod.2013.10.005

Delworth, T. L., & Greatbatch, R. J. (2000). Multidecadal thermohaline circulation variability driven by atmospheric surface flux forcing. *Journal of Climate*, *13*(9), 1481–1495. https://doi.org/10.1175/1520-0442(2000)013<1481:MTCVDB>2.0.CO;2

Drijfhout, S., van Oldenborgh, G. J., & Cimatoribus, A. (2012). Is a decline of AMOC causing the warming hole above the North Atlantic in observed and modeled warming patterns? *Journal of Climate*, *25*(24), 8373–8379. https://doi.org/10.1175/JCLI-D-12-00490.1

Dufresne, J.-L., Foujols, M.-A., Denvil, S., Caubel, A., Marti, O., Aumont, O., et al. (2013). Climate change projections using the IPSL-CM5 Earth system model: From CMIP3 to CMIP5. *Climate Dynamics*, *40*(9–10), 2123–2165. https://doi.org/10.1007/s00382-012-1636-1

Eden, C., & Willebrand, J. (2001). Mechanism of interannual to decadal variability of the North Atlantic circulation. *Journal of Climate*, *14*(10), 2266–2280. https://doi.org/10.1175/1520-0442(2001)014<2266:MOITDV>2.0.CO;2

Escudier, R., Mignot, J., & Swingedouw, D. (2013). A 20-year coupled ocean-sea ice-atmosphere variability mode in the North Atlantic in an AOGCM. *Climate Dynamics*, *40*(3-4), 619–636. https://doi.org/10.1007/s00382-012-1402-4

Fan, M., & Schneider, E. K. (2012). Observed decadal North Atlantic tripole SST variability. Part I: Weather noise forcing and coupled response. *Journal of the Atmospheric Sciences*, *69*(1), 35–50. https://doi.org/10.1175/JAS-D-11-018.1

Frankcombe, L. M., & Dijkstra, H. A. (2009). Coherent multidecadal variability in North Atlantic sea level. *Geophysical Research Letters*, *36*, L15604. https://doi.org/10.1029/2009GL039455

Frankcombe, L. M., & Dijkstra, H. A. (2011). The role of Atlantic-Arctic exchange in North Atlantic multidecadal climate variability. *Geophysical Research Letters*, *38*, L16603. https://doi.org/10.1029/2011GL048158

Frankcombe, L. M., Von Der Heydt, A., & Dijkstra, H. A. (2010). North Atlantic multidecadal climate variability: An investigation of dominant time scales and processes. *Journal of Climate*, *23*(13), 3626–3638. https://doi.org/10.1175/2010JCLI3471.1

Frankignoul, C., & Hasselmann, K. (1977). Stochastic climate models, part II Application to sea-surface temperature anomalies and thermocline variability. *Tellus*, *29*(4), 289–305.

Frankignoul, C., & Kestenare, E. (2002). The surface heat flux feedback. Part I: Estimates from observations in the Atlantic and the North Pacific. *Climate Dynamics*, *19*(8), 633–647.

Gastineau, G., D'Andrea, F., & Frankignoul, C. (2013). Atmospheric response to the North Atlantic Ocean variability on seasonal to decadal time scales. *Climate Dynamics*, *40*(9–10), 2311–2330. https://doi.org/10.1007/s00382-012-1333-0

Gastineau, G., & Frankignoul, C. (2012). Cold-season atmospheric response to the natural variability of the Atlantic Meridional Overturning Circulation. *Climate Dynamics*, *39*(1–2), 37–57. https://doi.org/10.1007/s00382-011-1109-y

Gastineau, G., L'hévéder, B., Codron, F., & Frankignoul, C. (2016). Mechanisms determining the winter atmospheric response to the Atlantic overturning circulation. *Journal of Climate*, *29*(10), 3767–3785. https://doi.org/10.1175/JCLI-D-15-0326.1

Grégorio, S., Penduff, T., Sérazin, G., Molines, J.-M., Barnier, B., & Hirschi, J. (2015). Intrinsic variability of the Atlantic Meridional Overturning Circulation at interannual-to-multidecadal time scales. *Journal of Physical Oceanography*, *45*(7), 1929–1946. https://doi.org/10.1175/JPO-D-14-0163.1

Griffies, S. M., Yin, J., Durack, P. J., Goddard, P., Bates, S. C., Behrens, E., et al. (2014). An assessment of global and regional sea level for years 1993–2007 in a suite of interannual CORE-II simulations. *Ocean Modelling*, *78*, 35–89. https://doi.org/10.1016/j.ocemod.2014.03.004

Häkkinen, S., & Rhines, P. B. (2004). Decline of subpolar North Atlantic circulation during the 1990s. *Science*, *304*(5670), 555–559. https://doi.org/10.1126/science.1094917

Hátún, H., Sandø, A. B., Drange, H., Hansen, B., & Valdimarsson, H. (2005). Influence of the Atlantic subpolar gyre on the thermohaline circulation. *Science*, *309*(5742), 1841–1844. https://doi.org/10.1126/science.1114777

Jackson, L. C., Kahana, R., Graham, T., Ringer, M. A., Woollings, T., Mecking, J. V., & Wood, R. A. (2015). Global and European climate impacts of a slowdown of the AMOC in a high resolution GCM. *Climate Dynamics*, *45*(11-12), 3299–3316. https://doi.org/10.1007/s00382-015-2540-2

Jamet, Q., Huck, T., Arzel, O., Campin, J.-M., & Colin de Verdière, A. (2016). Oceanic control of multidecadal variability in an idealized coupled GCM. *Climate Dynamics*, *46*(9–10), 3079–3095. https://doi.org/10.1007/s00382-015-2754-3

Jungclaus, J. H., Haak, H., Latif, M., & Mikolajewicz, U. (2005). Arctic–North Atlantic interactions and multidecadal variability of the meridional overturning circulation. *Journal of Climate*, *18*(19), 4013–4031. https://doi.org/10.1175/JCLI3462.1

Keenlyside, N. S., Latif, M., Jungclaus, J., Kornblueh, L., & Roeckner, E. (2008). Advancing decadal-scale climate prediction in the North Atlantic sector. *Nature*, *453*(7191), 84–88. https://doi.org/10.1038/nature06921

Knight, J. R., Folland, C. K., & Scaife, A. A. (2006). Climate impacts of the Atlantic multidecadal oscillation. *Geophysical Research Letters*, *33*, L17706. https://doi.org/10.1029/2006GL026242

Kwon, Y. O., & Frankignoul, C. (2012). Stochastically-driven multidecadal variability of the Atlantic Meridional Overturning Circulation in CCSM3. *Climate Dynamics*, *38*(5–6), 859–876. https://doi.org/10.1007/s00382-011-1040-2

Langehaug, H. R., Medhaug, I., Eldevik, T., & Otterå, O. H. (2012). Arctic/Atlantic exchanges via the subpolar gyre. *Journal of Climate*, *25*(7), 2421–2439. https://doi.org/10.1175/JCLI-D-11-00085.1

Madec, G. (2015). NEMO Ocean engine. *Note Du Pôle de Modélisation, Institut Pierre Simon Laplace, France, Technical Report, 27*.

McCarthy, G., Frajka-Williams, E., Johns, W. E., Baringer, M. O., Meinen, C. S., Bryden, H. L., et al. (2012). Observed interannual variability of the Atlantic Meridional Overturning Circulation at 26.5°N. *Geophysical Research Letters*, *39*, L19609. https://doi.org/10.1029/2012GL052933

Meehl, G. A., Goddard, L., Boer, G., Burgman, R., Branstator, G., Cassou, C., et al. (2014). Decadal climate prediction: An update from the trenches. *Bulletin of the American Meteorological Society*, *95*(2), 243–267. https://doi.org/10.1175/BAMS-D-12-00241.1

Menary, M. B., Hodson, D. L., Robson, J. I., Sutton, R. T., Wood, R. A., & Hunt, J. A. (2015). Exploring the impact of CMIP5 model biases on the simulation of North Atlantic decadal variability. *Geophysical Research Letters*, *42*, 5926–5934. https://doi.org/10.1002/2015GL064360

Mercier, H., Lherminier, P., Sarafanov, A., Gaillard, F., Daniault, N., Desbruyères, D., et al. (2015). Variability of the meridional overturning circulation at the Greenland–Portugal OVIDE section from 1993 to 2010. *Progress in Oceanography*, *132*, 250–261. https://doi.org/10.1016/j.pocean.2013.11.001

Mignot, J., & Frankignoul, C. (2005). The variability of the Atlantic Meridional Overturning Circulation, the North Atlantic oscillation, and the El Niño–Southern Oscillation in the Bergen climate model. *Journal of Climate*, *18*(13), 2361–2375. https://doi.org/10.1175/JCLI3405.1

Mignot, J., García-Serrano, J., Swingedouw, D., Germe, A., Nguyen, S., Ortega, P., et al. (2016). Decadal prediction skill in the ocean with surface nudging in the IPSL-CM5A-LR climate model. *Climate Dynamics*, *47*(3–4), 1225–1246. https://doi.org/10.1007/s00382-015-2898-1

Muir, L., & Fedorov, A. (2015). How the AMOC affects ocean temperatures on decadal to centennial timescales: The North Atlantic versus an interhemispheric seesaw. *Climate Dynamics*, *45*(1–2), 151–160. https://doi.org/10.1007/s00382-014-2443-7

Muir, L. C., & Fedorov, A. V. (2017). Evidence of the AMOC interdecadal mode related to westward propagation of temperature anomalies in CMIP5 models. *Climate Dynamics*, *48*(5–6), 1517–1535. https://doi.org/10.1007/s00382-016-3157-9

Ortega, P., Mignot, J., Swingedouw, D., Sévellec, F., & Guilyardi, E. (2015). Reconciling two alternative mechanisms behind bi-decadal variability in the North Atlantic. *Progress in Oceanography*, *137*, 237–249. https://doi.org/10.1016/j.pocean.2015.06.009

Peings, Y., & Magnusdottir, G. (2014). Forcing of the wintertime atmospheric circulation by the multidecadal fluctuations of the North Atlantic Ocean. *Environmental Research Letters*, *9*(3), 034018. https://doi.org/10.1088/1748-9326/9/3/034018

Peings, Y., Simpkins, G., & Magnusdottir, G. (2016). Multidecadal fluctuations of the North Atlantic Ocean and feedback on the winter climate in CMIP5 control simulations. *Journal of Geophysical Research: Atmospheres*, *121*, 2571–2592. https://doi.org/10.1002/2015JD024107

Plaut, G., Ghil, M., & Vautard, R. (1995). Interannual and interdecadal variability in 335 years of central England temperatures. *Science*, *268*(5211), 710–713. https://doi.org/10.1126/science.268.5211.710

Rahmstorf, S. (2002). Ocean circulation and climate during the past 120,000 years. *Nature*, *419*(6903), 207–214. https://doi.org/10.1038/nature01090

Rahmstorf, S., Box, J. E., Feulner, G., Mann, M. E., Robinson, A., Rutherford, S., & Schaffernicht, E. J. (2015). Exceptional twentieth-century slowdown in Atlantic Ocean overturning circulation. *Nature Climate Change*, *5*(5), 475–480. https://doi.org/10.1038/nclimate2554

Schneider, E. K., & Fan, M. (2007). Weather noise forcing of surface climate variability. *Journal of the Atmospheric Sciences*, *64*(9), 3265–3280. https://doi.org/10.1175/JAS4026.1

Sérazin, G., Meyssignac, B., Penduff, T., Terray, L., Barnier, B., & Molines, J.-M. (2016). Quantifying uncertainties on regional sea level change induced by multidecadal intrinsic oceanic variability. *Geophysical Research Letters*, *43*, 8151–8159. https://doi.org/10.1002/2016GL069273

Servonnat, J., Mignot, J., Guilyardi, E., Swingedouw, D., Séférian, R., & Labetoulle, S. (2015). Reconstructing the subsurface ocean decadal variability using surface nudging in a perfect model framework. *Climate Dynamics*, *44*(1–2), 315–338. https://doi.org/10.1007/s00382-014-2184-7

Sévellec, F., & Fedorov, A. V. (2010). Excitation of SST anomalies in the eastern equatorial Pacific by oceanic optimal perturbations. *Journal of Marine Research*, *68*(3), 597–624. https://doi.org/10.1357/002224010794657092

Sévellec, F., & Fedorov, A. V. (2013). The leading, interdecadal eigenmode of the Atlantic Meridional Overturning Circulation in a realistic ocean model. *Journal of Climate*, *26*(7), 2160–2183. https://doi.org/10.1175/JCLI-D-11-00023.1

Smeed, D. A., McCarthy, G. D., Cunningham, S. A., Frajka-Williams, E., Rayner, D., Johns, W. E., et al. (2014). Observed decline of the Atlantic Meridional Overturning Circulation 2004–2012. *Ocean Science*, *10*(1), 29–38. https://doi.org/10.5194/os-10-29-2014

Stouffer, R. J., Yin, J., Gregory, J. M., Dixon, K. W., Spelman, M. J., Hurlin, W., et al. (2006). Investigating the causes of the response of the thermohaline circulation to past and future climate changes. *Journal of Climate*, *19*(8), 1365–1387. https://doi.org/10.1175/JCLI3689.1

Swingedouw, D., Mignot, J., Braconnot, P., Mosquet, E., Kageyama, M., & Alkama, R. (2009). Impact of freshwater release in the North Atlantic under different climate conditions in an OAGCM. *Journal of Climate*, *22*(23), 6377–6403. https://doi.org/10.1175/2009JCLI3028.1

Te Raa, L. A., & Dijkstra, H. A. (2002). Instability of the thermohaline ocean circulation on interdecadal timescales. *Journal of Physical Oceanography*, *32*(1), 138–160. https://doi.org/10.1175/1520-0485(2002)032<0138:IOTTOC>2.0.CO;2

Timmermann, A., Latif, M., Voss, R., & Grötzner, A. (1998). Northern hemispheric interdecadal variability: A coupled air–sea mode. *Journal of Climate*, *11*(8), 1906–1931. https://doi.org/10.1175/1520-0442-11.8.1906

Vellinga, M., & Wood, R. A. (2002). Global climatic impacts of a collapse of the Atlantic thermohaline circulation. *Climatic Change*, *54*(3), 251–267. https://doi.org/10.1023/A:1016168827653

Wen, N., Frankignoul, C., & Gastineau, G. (2016). Active AMOC–NAO coupling in the IPSL-CM5A-MR climate model. *Climate Dynamics*, *47*(7–8), 2105–2119. https://doi.org/10.1007/s00382-015-2953-y

Zhang, R. (2017). On the persistence and coherence of subpolar sea surface temperature and salinity anomalies associated with the Atlantic multidecadal variability. *Geophysical Research Letters*, *44*, 7865–7875. https://doi.org/10.1002/2017GL074342